

**DESIGN AND ANALYSIS OF A SELF-BALANCING TWO-WHEEL VEHICLE
ATTACHMENT USING MECHANICAL GYROSCOPES**

A Final Year Project Report

Presented to

SCHOOL OF MECHANICAL & MANUFACTURING ENGINEERING

Department of Mechanical Engineering

NUST

ISLAMABAD, PAKISTAN

In Partial Fulfillment

of the Requirements for the Degree of
Bachelor of Mechanical Engineering

by

Hassan Ali Khan

Mahad Niazi

Roha Ashfaq

Wasif Rehman

June 2021

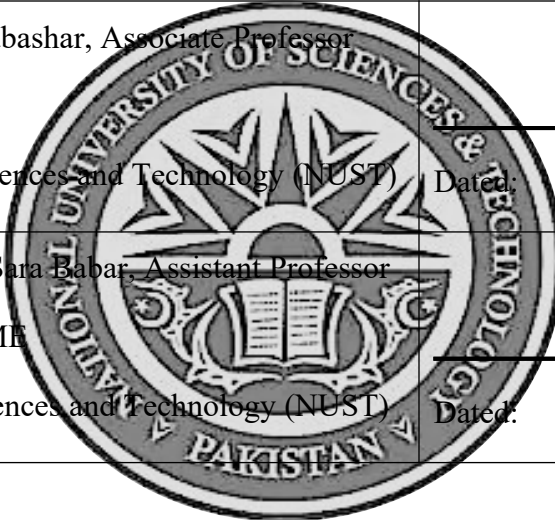
EXAMINATION COMMITTEE

We hereby recommend that the final year project report prepared under our supervision by:

HASSAN ALI KHAN	209946
MAHAD NIAZI	207996
ROHA ASHFAQ	208451
WASIF REHMAN	221388

Titled: "DESIGN AND ANALYSIS OF A SELF-BALANCING TWO-WHEEL VEHICLE USING MECHANICAL GYROSCOPE" be accepted in partial fulfillment of the requirements for the award of BACHELOR OF MECHANICAL ENGINEERING degree with grade _____

Supervisor: Dr. Aamir Mubashar, Associate Professor SMME National University of Sciences and Technology (NUST)	Dated: _____
Committee Member: Dr. Sura Babar, Assistant Professor SMME National University of Sciences and Technology (NUST)	Dated: _____



(Head of Department)

(Date)

COUNTERSIGNED

Dated: _____

(Dean / Principal)

ABSTRACT

A self-balancing mechanism is designed for enhancing locally produced motorcycles' handling by using a mechanical gyroscope. Gyroscope is a spinning wheel which has a considerable mass, having high angular velocity, which when tilted, generates a force perpendicular to the actual motion of the body and its direction is determined by the direction in which the mass rotates and tilts. This produced force will be utilized to balance the body roll of the motorbike, hence keeping it stable. Rotation of vertical pair of gyroscopes is achieved using a hub motor which will draw its power supply from a separately attached 48V Li-ion battery. To ensure the accurate response of gyroscope, according to tilt of bike, closed loop stability is achieved by designing a control system. To accurately design the control system, Dynamic model of the bike-gyroscope system needs to be derived. Equations of motion for the system have been derived using the Euler-Langrange method and later numerical techniques such as Runge-Kutta 4 method were adopted to solve the system. In terms of structural modelling, a 3D model containing a pair of gyroscopes has been designed along with the two hub motors in a bench. To ensure that the model does not fail mechanically during its working; stress, acceleration and vibrational analysis have been performed, respectively. Ultimately, the designs fulfill the purpose of rider safety, by balancing the motorcycle.

ACKNOWLEDGEMENTS

First and foremost, we would like to thank Allah Almighty for giving us the heart and mind to pursue this project and take it to completion. Our heartfelt gratitude goes out to our supervisor, Dr. Aamir Mubashar, for his relentless support, guidance. We specially appreciate his generosity in terms of him sparing his time for meeting with us and providing us his valuable feedback throughout the length of the project.

We would also like to convey our acknowledgements to Lecturer Shoaib Ahmed in aiding us in our mathematical modelling as well as Sir Husnain, Lecturer Danyal Zahid and Dr. Sara Baber for their effort in helping us find our way. We would like to thank all the authors and relevant online libraries for aiding us in drafting this report.

We would like to acknowledge our families and friends for their unconditional love and all kinds of support for the duration of this degree without which we would not have made it this far. Special thanks to our batchmates Mr. Zun Nooren Bangash and Mr. Saad Ejaz, and our senior Mr. Ali Ahmar for their timely support throughout the duration of this project.

ORIGINALITY REPORT

Table of Contents

ABSTRACT.....	ii
ACKNOWLEDGEMENTS.....	iii
ORIGINALITY REPORT.....	iv
LIST OF FIGURES.....	viii
LIST OF TABLES.....	x
ABBREVIATIONS.....	xi
NOMENCLATURE.....	xii
CHAPTER 1: INTRODUCTION.....	1
1.1 Problem Identification.....	1
1.2 Motivation.....	1
1.3 Objectives.....	2
1.4 Aim.....	2
1.5 Scope.....	2
CHAPTER 2: LITERATURE REVIEW.....	4
2.1 Introduction.....	4
2.2 Current Progress in Deriving Safety Features.....	4
2.3 Self-Balancing Design.....	6
2.4 Mathematical Modelling.....	8
2.5 Controller Design.....	10
CHAPTER 3: METHODOLOGY.....	12
3.1 Equations of Motion.....	12
3.2 Gyroscope Design.....	22
3.2.1 Size Optimizations.....	23
3.3 Solutions of the Controlled System.....	24
3.3.1 Plots.....	27
3.3.2 Discussion.....	28
3.4 Self-Balancing Action of the Control Moment Gyroscope System: 29	29

3.4.1	Stability Analysis of the Uncontrolled System:.....	31
3.4.2	Analysis of Proportional Integral Derivative (PID) Controlled System:.....	35
3.4.3	Actuation Procedure.....	41
3.5	Mechanism Design Process.....	41
3.5.1	Initial Designs.....	42
3.6	Final Design.....	43
3.6.1	Model Views.....	44
3.6.2	Part Dimensions.....	49
3.6.3	Bolts Specification.....	51
3.6.4	Nuts Specifications.....	51
3.6.5	Bearings Specifications.....	51
3.6.6	Material Selection.....	51
3.7	Prototyping Cost Details.....	52
3.8	Summary.....	53
	CHAPTER 4: RESULTS AND DISCUSSIONS.....	54
4.1	Introduction.....	54
4.2	Part Analysis.....	54
4.2.1	Main Frame.....	55
4.4.2	Support Bracket.....	59
4.4.3	Gyroscope Attachment.....	62
4.3	Assembly Analysis.....	64
	CHAPTER 5: CONCLUSIONS AND RECOMMENDATIONS.....	68
	REFERENCES.....	70
	APPENDIX I: PYTHON CODE FOR CONTROLLED SYSTEM.....	72
	APPENDIX II: RK ORDER 4 METHOD CODE.....	79
	APPENDIX III: MATLAB CODE FOR CONTROLLER.....	82
	APPENDIX IV: CONTROLLER PARAMETERS.....	84
	APPENDIX V: BILL OF MATERIALS.....	85

APPENDIX VI: BEARING DIMENSIONS.....	86
APPENDIX VII: DETAILED PART DRAWINGS.....	87

LIST OF FIGURES

Figure 1: Number of Accidents by Vehicle Type.....	4
Figure 2: Honda Rider Assist.....	5
Figure 3: Lit Motors' C-1.....	5
Figure 4: Existing Experimental Setup.....	6
Figure 5: Existing Experimental Setup 2	7
Figure 6: Zero Propellant maneuvers for ISS by using 4 double-gimbal parallel-mounted CMGs [13].....	8
Figure 7: Roll angle of the Motorcycle.....	12
Figure 8: Tilt Angle of the Gyroscope.....	12
Figure 9: Combined Plot.....	27
Figure 10: Theta vs Time.....	27
Figure 11: Alpha vs Time.....	27
Figure 12: Torque vs Time.....	27
Figure 13: Voltage vs Time.....	28
Figure 14: Current vs Time.....	28
Figure 15: Energy vs Time.....	28
Figure 16: Power vs Time.....	28
Figure 17: Pole Zero Plot.....	32
Figure 18: Pole Zero Plot (Zoomed).....	33
Figure 19: Bode Plot.....	34
Figure 20: Step Response.....	34
Figure 21: Control System Block Diagram.....	35
Figure 22: Step Plot - Reference Tracking.....	36
Figure 23: Controlled System's Bode Plot.....	38
Figure 24: Input Disturbance Rejection.....	38
Figure 25: Output Disturbance Rejection.....	39
Figure 26: Controller Effort.....	39
Figure 27: Controlled System's Pole Zero Plot.....	40
Figure 28: Controlled System's Pole Zero Plot (Zoomed).....	40
Figure 29: Physical Actuation Procedure.....	41
Figure 30: Initial Design Two Vertical Gyroscopes beneath Motorbike Frame.....	42
Figure 31: 3D Simplified Model of Initial Design.....	42
Figure 32: Initial Design with Single Vertical Gyroscope.....	43
Figure 33: Initial Design with Single Horizontal Gyroscope.....	43
Figure 34: Isometric View of Model.....	44
Figure 35: Modelling Design SolidWorks.....	45
Figure 36: Assembly Side View.....	45
Figure 37: Assembly Front View.....	46
Figure 38: Assembly Top View.....	46

Figure 39: Assembly Exploded View.....	47
Figure 40: Side View Hub Motor.....	47
Figure 41: Hub Motor 3D View.....	48
Figure 42: Hub Motor Exploded View.....	48
Figure 43: 3D Model View.....	49
Figure 44: Model Placement on Vehicle.....	49
Figure 45: Drawing Specifications.....	50
Figure 46: Main Frame Coarse Meshing.....	55
Figure 47: Main Frame Fine Meshing.....	56
Figure 48: Frame Von Mises Stress Analysis.....	56
Figure 49: Main Frame Strain Analysis.....	57
Figure 50: Main Frame Strain Analysis Close-up.....	57
Figure 51: Main Frame Vibrational Stress Analysis.....	58
Figure 52: Main Frame Vibrational Strain Analysis.....	58
Figure 53: Support Bracket Coarse Mesh.....	59
Figure 54: Support Bracket Fine Mesh.....	60
Figure 55: Support Bracket Stress Analysis.....	60
Figure 56: Support Bracket Strain Analysis.....	61
Figure 57: Support Bracket Vibrational Stress.....	61
Figure 58: Gyroscope Coarse Mesh.....	62
Figure 59: Gyroscope Fine Mesh.....	63
Figure 60: Gyroscope Stress Simulation at High Speeds.....	63
Figure 61: Gyroscope Strain Analysis at High Speeds.....	63
Figure 62: Gyroscope Vibrational Stress Analysis.....	64
Figure 63: Coarse Mesh Assembly.....	65
Figure 64: Fine Mesh Assembly.....	65
Figure 65: Displacement Magnitude (m).....	66
Figure 66: Velocity Magnitude.....	66
Figure 67: Von Mises Stress.....	67

LIST OF TABLES

Table 1: Parameters and their Values.....	30
Table 2: Controller Parameters.....	37
Table 3: Controller Performance and Robustness.....	37
Table 4: Bolt Specifications.....	51
Table 5: Nuts Specifications.....	51
Table 6: Specifications of Stainless Steel AISI 4340.....	52
Table 7: Bill of Materials.....	85
Table 8: 6000 Ball Bearing Properties.....	86

ABBREVIATIONS

FPGA	Field Programmable Gate Array
CMG	Control Moment Gyroscope
IMU	Inertial Measurement Unit
ABS	Anti-Lock Braking System
ADAS	Advanced Driver Assistance System
ISS	International Space Station
RK4	Runge Kutta Order 4
FEA	Finite Element Analysis
DOF	Degrees of Freedom
MOI	Moment of Inertia
COG	Center of Gravity

NOMENCLATURE

m_g	Mass of Gyroscope
m_b	Mass of Motorbike
r	Pivot Point of gyro from ground
l	COG of gyro from pivot point
H	Motorbike COG upright height
I_b	Motorbike moment of inertia around ground contact line
$I_{\varphi\varphi}$	Flywheel polar moment of inertia around COG
$I_{\alpha\alpha}$	Flywheel radial moment of inertia around COG
ω	Flywheel angular velocity
L	Motor Inductance
R	Motor Resistance
K_t	Motor torque constant
K_e	Motor back emf constant
α	Gyroscope 1 tilt angle
β	Gyroscope 2 tilt angle
θ	Tilt angle of the motorbike

CHAPTER 1: INTRODUCTION

1.1 Problem Identification

In a developing country such as Pakistan where the majority of people are poor and barely make ends meet, personal means of transport is nothing less than a luxury. A car no less, is an even more luxurious item and only some people within Pakistan can afford to buy and maintain one. So naturally, a two-wheeler motorcycle is the much-preferred vehicular transport bought by many locals as it is cheaper to buy and operate. However, with this rise in the number of motorcyclists in our country, there comes a drastic rise in road accidents resulting in injuries and deaths.

1.2 Motivation

In Pakistan, 71% of road accidents are motorcycle accidents [1] which can be attributed to the intrinsic lack of safety while driving a motorbike combined with the inferior safety standards of motorbikes available in Pakistan. As of 2014, motorcycles accounted for 68.2% of the total number of registered vehicles [2]. Since then, the number has only increased. There is a dire need to improve the safety standards of these motorcycles at an economical expense in order to diminish the chances of meeting with an accident while riding in a motorcycle.

Another important issue in Pakistan is the prevalence of locomotor diseases such as Polio. These diseases affect the ability of the person it affects to walk and operate transport vehicles in general. The prevalence of locomotor disease around the world is around 2.08% [3] and on top of that, many people lose their lower limbs due to numerous other reasons [4]. Loss of lower limb seriously affects the lifestyle of the affected people and can hinder them from routine work like commuting, reporting to their workplace etc. Almost every job requires you to be available in person and to do tasks that involve meeting people and commuting to different areas for different reasons. People that have suffered from the above-mentioned circumstances find it very difficult to fit in and usually have to let go of their stable income and their livelihood.

1.3 Objectives

Catering to the above two important issues, a solution was devised in the form of a self-balancing motorcycle. This self-balancing action would not only improve the general handling of the motorcycle especially at low speeds, but also cater to the group of people affected by locomotor disease and as it will remain balanced throughout the ride without any additional support. In the past, a wheel attachment is attached to the motorbike for such people, but this reduces the maneuverability of the motorcycle and increases the motorbike's turning radius.

The self-balancing bike will be designed using a control moment gyroscope which generally consists of a rotating flywheel and a motorized gimbal that tilts the rotating flywheel which in turn creates a torque that will be felt by the frame that supports it. Hence, this precessional torque produced by the tilt of the rotating flywheels will in turn provide the balancing torque to the oppose the tilt of the motorbike and keep it balanced.

The tilt of the rotating flywheel will depend on the tilt of the motorbike from its perpendicular axis and a correlation has to be built between the two with the help of a control system so that the tilt action of the gyroscope counters the tilt of the motorbike and as the angle of the motorbike reduces, so does the angle of the tilt of the gyroscope such that it becomes zero when then the motorbike stabilizes.

1.4 Aim

The project aims to provide a self-balancing aid to the motorcycles that are in production in Pakistan. This attachment will remarkably improve the handling of the motorcycles, especially at low speeds and will provide as a means for transportation for the handicapped population. In short, we aim to:

“Design a self-balancing attachment for existing motorcycles that can balance the motorbike from an initial roll angle of as much as 17° from the mean position.”

1.5 Scope

The scope of this project covers the following main deliverables:

1. Engineer the dynamics model of the motorbike.
2. Design a controller to balance the motorbike using the dynamics model.

3. Design a 3D model of the gyroscope attachment.
4. Perform Structural Simulation of the 3D Model.
5. Perform Vibrational Analysis on the 3D Model.

CHAPTER 2: LITERATURE REVIEW

2.1 Introduction

As discussed earlier, there is a prevalent association between motorcycling and greater danger of crash frequency and deaths than cars. The following figure representing a dataset collected by Akhtar et al. supports this claim [1].

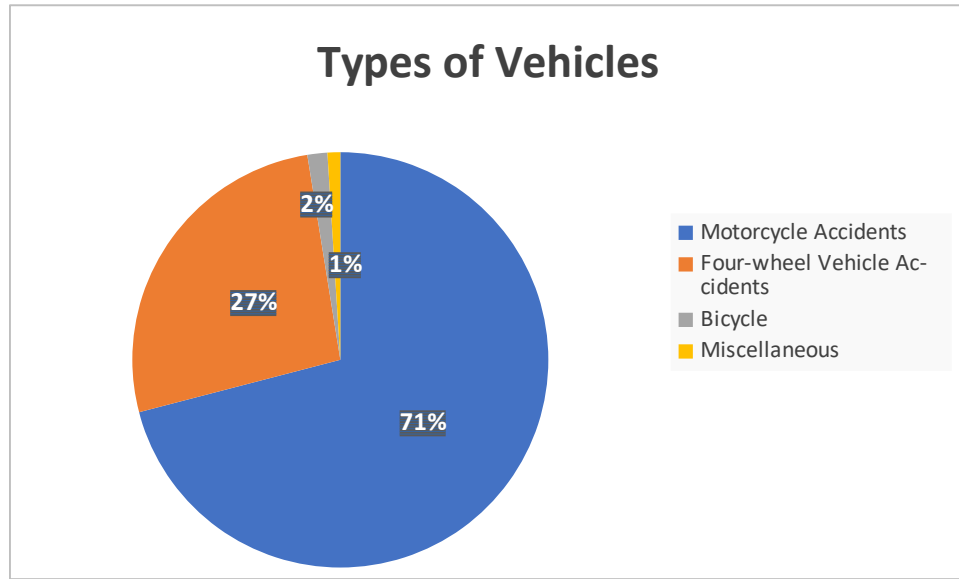


Figure 1: Number of Accidents by Vehicle Type

Justifiably, a lot of work has recently been done internationally on introducing different safety features for motorcycles. Some notable mentions include Advanced Driver Assistance Systems (ADAS), ABS, Brake Assist, and Collision Warning and Avoidance Systems [5]. However, none of these features find its application in locally manufactured motorcycles here in Pakistan as these safety features can directly increase the cost of these motorbikes and make it unaffordable for many.

2.2 Current Progress in Deriving Safety Features

Motorcycles are widely used in Pakistan due to their:

- a) Low buying and running cost.
- b) High maneuverability in crammed up spaces.

Motorcycles' innate lack of safety can be attributed to the absence of natural stability like a car. However, the lack of four wheels spread over a wide area is also what makes it so

easy to maneuver in narrow streets and in high traffic settings. Hence, companies are working on devising a self-balancing solution that would give the motorbike the stability of 4 wheels all the while keeping its maneuverability intact.

Figure 2 and Figure 3 below are some of the solutions that tackle self-balancing. However, these existing solutions are relatively expensive and are not affordable by the public here in Pakistan. Honda Rider Assist has not yet been commercialized and is still in its experimental stage, however, the estimated price is placed at around PKR 3,000,000. Similarly, Lit Motors' C1 is to be approximately priced at PKR 3,697,200. Both these prices are ex-factory and will be subjected to duty and other charges once imported to Pakistan.



Figure 2: Honda Rider Assist



Figure 3: Lit Motors' C-1

Its target demographic belongs to the upper class and evidently, the majority of the population of Pakistan cannot afford such an expense.

This is the problem this project tackles, it aims to provide a rudimentary self-balancing technology in our locally produced motorcycles at the fraction of the cost at which they are available internationally. We believe that this sort of technology will not only help improve the safety of two-wheeled motorbikes for the public but will also function as a mode of transport for the less fortunate people who have lost a limb or suffer from a locomotor disease.

2.3 Self-Balancing Design

Self-balancing of an equipment can be achieved in various ways. To find the most ideal design other methods were reviewed in the initial stages of this project such as the use of gyroscopic stabilization by Beznos et al. [6]. This stabilization procedure entailed using two coupled gyroscopes spinning in opposite direction which stabilized the bicycle using the precessional torque of the gyroscopes. This became an inspiration for this project's design of two coupled rotating flywheels.

The first design that was found to exist in experimentation stage consisted of a single vertical gyroscope that would provide torque for balancing while being attached to the front of the motorcycle.



Figure 4: Existing Experimental Setup

The next design that was also an experimental test bench. It consisted of a single gyroscope oriented along horizontal axis and it was placed at the back of the vehicle.



Figure 5: Existing Experimental Setup 2

Lee and Ham in 2002 [7] came up with a control strategy based on a load mass balance system which proposed “*to turn and move the bicycle system left and right by controlling the center of load mass left and right respectively*”.

There were other works like using steering control to balance a bicycle [8] and balancing the bicycle by controlling the magnitude of torque exerted on the steering handlebar using gyro stabilization [9] but they were not as relevant to the problem at hand.

Among these methods, it was found that using CMG is the ideal choice as it is relatively quick [10] and provides a substantial amount of torque that can balance motorbike which is relatively heavy [11]. Another advantage other than the production of large amount of torque is that it has no ground reaction force [12]. Currently CMGs are majorly used in maneuver and control of large spacecrafts and satellites including the ISS. However, recently some work was done by Lam [12] to implement CMG on a smaller scale rather than its conventional use in the larger satellite market.

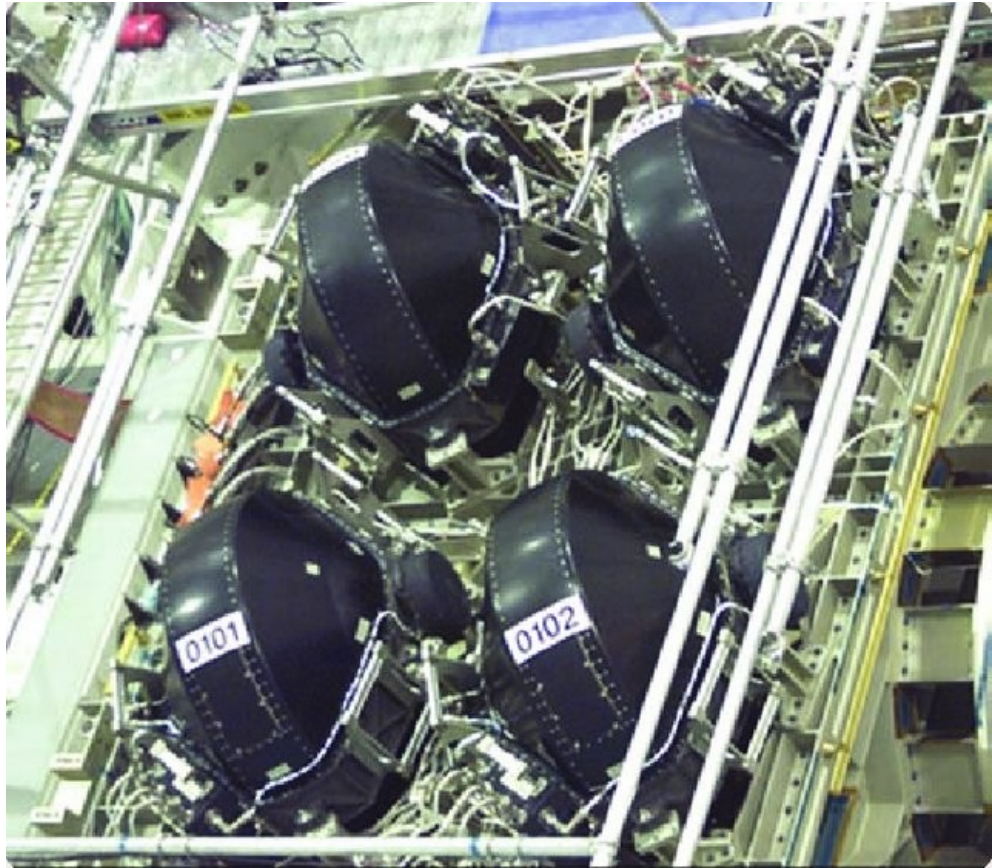


Figure 6: Zero Propellant maneuvers for ISS by using 4 double-gimbal parallel-mounted CMGs [13]

Since a larger torque value per unit kg is required on top of the stability of the motorcycle when it is stationary. Hence, the Control Moment Gyro technique will be employed to help the motorbike achieve ‘self-balancing’.

2.4 Mathematical Modelling

First and foremost, to designing a control system for the CMG, the equations of motion for the entire gyroscope-motorbike design have to be derived. There are multiple methods for deriving equations of motion, three of them are of particular interest which include Newton equations of motion, Lagrangian equations of motion and Hamiltonian equations of motion.

1. Newton equations of motion rely on vector-based approach of finding vector sum of forces and equating it to mass times acceleration. But Newton approach requires to find constraint forces. Also, finding equations of motions in other coordinate systems is much harder using Newton equations of motions [14].

2. Lagrangian equations of motion is scalar approach as it is based on energy of system. So, it is easier to find equations of motions of constraint systems without finding constraint forces and finding equations of motions in other coordinate systems is also easier. But as finding the energy function of dissipative forces is relatively complex and difficult, thus frictional effects are difficult to account using energy-based approaches in general [14].
3. Hamiltonian equations of motion gives same benefits as that of Lagrangian equations of motions as they also are energy based and it is easy to find equations of motions in other coordinate systems. However, rather than trying to describe system in terms of generalized coordinates and generalized velocities they try to describe the system in term of generalized coordinates and generalized momentums. This does not offer any significant advantage over Lagrangian equations of motions. Moreover, the algebra is more complicated in Hamiltonian equations of motions as in this case as there are variables involved in the denominator [14].

Thus, Lagrangian method was more suitable than the other two methods of deriving the equations of motion. All the modern relevant research papers indicated that the Lagrangian equations of motions be employed for gyroscopic balance of two-wheeler.

For stabilizing the motorbike, the torque has to be exerted by the gyroscopes such as to produce the stabilization effect on the motorbike. Such a torque can be found in multiple ways. Some of them are discussed below:

1. Assumptions about other nature coordinates can be made to solve system of differential to find required torque acting on the gyroscope to balance the motorbike. Necessary coordinates on which assumptions can be imposed are tilt angle of motorbike (θ), velocity associated with this tilt of the motorbike ($\dot{\theta}$), the tilt angle of gyroscopes (α and β) and corresponding rotational velocities ($\dot{\alpha}$ and $\dot{\beta}$). Among these six coordinates, conditions on motorbike tilt angle and gyroscope tilt velocities are discussed below:
 - a) Tilt of motorbike was assumed to follow certain function and a system of differential equations is solved for corresponding gyroscope tilt and torque on the gyroscope. This method will transform the differential equation to

a boundary value problem so schemes such as finite difference method has to be applied. Due to this reason, it is more computationally expensive and was not discussed in the text.

- b) As discussed above, certain conditions on gyroscope's tilt velocities along with some assumption convert differential equation of motorbike tilt angle (θ) to second order differential equation with motion similar to that of simple harmonic motion. This results in solution problem be converted to a much simpler initial value problem as compared to first method and is less computationally expensive, which is also the reason it is discussed in the text [15].
- 2. PID controllers can be used to determine required voltage applied across the motor circuit. The motor then exerts torque on the gyroscopes to tilt the rotating masses as to balance the motorbike. This was also discussed in the text [15].

Derivation of equations of motions lead to a system of nonlinear second order differential equations. Solving this system of equations analytically was not suitable so numerical schemes had to be employed to solve such differential equations. There are many numerical algorithms used to solve initial value problems such as Euler and Runge-Kutta algorithms etc., but Runge-Kutta method of order 4 is more accurate and easier to implement compared to other methods. So, it was preferred over other numerical methods for solving differential equations [16].

2.5 Controller Design

Following the dynamic modelling, a controller needs to be designed to provide the balancing torque within milliseconds of induced body roll of the motorbike. First off, a controller type had to be chosen from the options of PI, PD and PID controllers. From extensive research it was found that PID was the most suitable candidate. PI controllers were found to be better at the ability to track setpoints and had negligible steady state errors. Same was not the case for a PD controller and it persistently gave a higher steady state error. As good control was required for the case of the self-balancing motorcycle, PD controller was not a wise choice. Now for PI controller, the overshoot percentage is generally greater than that of a PD and a PID controller. PID controller not only provided a negligible steady state error, had a lower overshoot percentage when compared to a PI,

but also had the fastest time constant and settling time [17]. This made it an obvious choice for the case of self-balancing motorcycle attachment.

CHAPTER 3: METHODOLOGY

3.1 Equations of Motion

This project aims to employ a control moment gyroscope (CMG) which is an attitude control device used in modern spacecraft maneuver systems. It entails a circular disk (flywheel) which rotates continuously about its center attached with a servo motor at one end that tilts the rotating flywheel, in turn changing the angular momentum that produces a precessional torque which ultimately rotates/maneuvers the spacecraft as required [18].

For the purpose of this project, it was found that it would be more ideal to use two such spinning rotors, each attached with a motorized gimbal to provide the necessary precessional torque to balance the motorbike as it tilts.

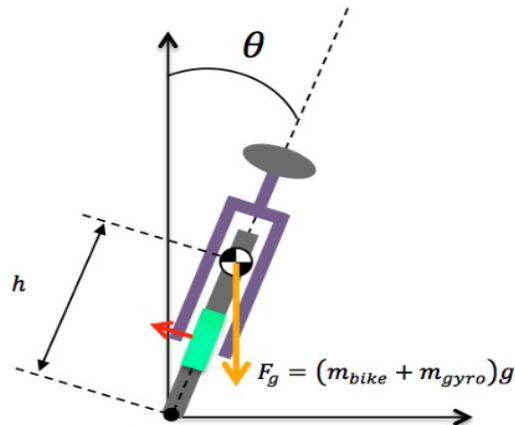


Figure 7: Roll angle of the Motorcycle

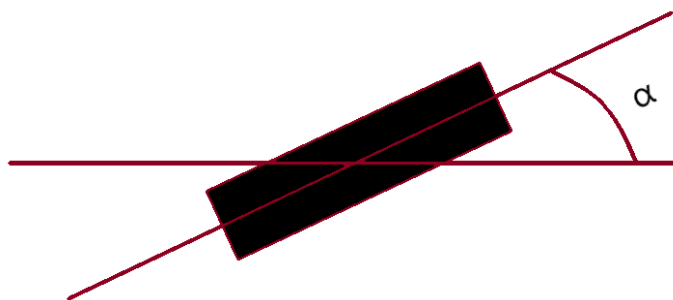


Figure 8: Tilt Angle of the Gyroscope

As the motorbike tilts by an angle θ as shown in Figure 7, an IMU will sense the body roll angle of the motorbike instantaneously. This data calculated by the IMU is then fed into the attached controller that gives out a certain voltage to the servo motor attached to the gimbal of the rotors to produce a tilt ' α ' on the continuously rotating flywheels as shown in Figure 8. This tilt action eventually balances the motorbike and reduces θ of the motorbike to zero.

To design the control system for balancing, the behavior of motorbike-gyroscope system was needed to be understood. Thus, it is necessary to derive the equations of motion for the motorbike-gyroscope system as they give insight into the behavior of the system. Equations of motion also help determining the stability of system under different control responses. Equations of motion can be derived using Newton Second law, Euler-Lagrange equations, or Hamiltonian equations. As gyroscopes are constraint to move along a certain axis, so there are internal forces that are hard to determine. Hence, deriving equations using the Newton's Second law is much more complex and difficult as compared to Euler-Lagrange equations. The algebra is messier and difficult to comprehend for Hamiltonian equations as variables appear in denominator. This makes Lagrange equations the most viable mode of derivation as compared to others as it avoids constraint forces and is easier than the Hamiltonian approach.

Consider a motorbike of mass m_b in global xyz-coordinate system which is oriented at angle θ with respect to the vertical. The first gyroscope of mass $m_{g,1}$ is oriented at an angle α with respect to the vertical in the local coordinate system of motorbike and is spinning with the angular velocity of ϕ . In a similar manner, β is defined for the second gyroscope of mass $m_{g,2}$ which is spinning with an angular velocity ψ . Let ' r_1 ' and ' r_2 ' be the distances from ground to pivot of the first gyroscope and second gyroscope, respectively. ' l_1 ' and ' l_2 ' are defined as the distance from respective gyroscope's pivot to its center of mass. Thus, the vertical height of first gyroscope's center of mass from ground is

$$h_{g,1} = (r_1 + l_1 \cos \alpha) \cos \theta \quad (3.1)$$

And the height of the second gyroscope's center of mass from ground is

$$h_{g,2} = (r_2 + l_2 \cos \beta) \cos \theta \quad (3.2)$$

Similarly, if 'H' is the distance from ground to center of mass of motorbike, then the vertical height from the center of mass to ground after tilting by angle θ from the vertical is given by

$$h_b = H \cos \theta \quad (3.3)$$

Thus, the total potential energy of motorbike-gyroscope system is

$$V = V_b + V_{g,1} + V_{g,2} \quad (3.4)$$

Substituting the values of V_b , $V_{g,1}$ and $V_{g,2}$ in the above equation yields

$$V = m_b g H \cos \theta + m_{g,1} g (r_1 + l_1 \cos \alpha) \cos \theta + m_{g,2} g (r_2 + l_2 \cos \beta) \cos \theta \quad (3.5)$$

Gyroscope's total kinetic energy is the sum of kinetic energy of gyroscope's center of mass and the kinetic energy of gyroscope about the center of mass [14].

$$T_{g,1} = \int_R \frac{1}{2} v'_{i,1} dm + \frac{1}{2} m_{g,1} v_{g,1cm}^2 \quad (3.6)$$

here $v'_{i,1}$ is the velocity of infinitesimal mass of first gyroscope 'dm' relative to center of mass, and $v_{g,1cm}$ is velocity of the center of mass of the first gyroscope. For a rigid gyroscope, equation 3.6 can be rewritten in the form

$$T_{g,1} = \frac{1}{2} \omega_1^T I_{1,cm} \omega_1 + \frac{1}{2} m_{g,1} v_{g,1cm}^2 \quad (3.7)$$

here $I_{1,cm}$ is the moment of inertial tensor of first gyroscope about its center of mass and ω_1 is instantaneous angular velocity vector of the first gyroscope. The moment of inertial tensor has nine components but along the principal axis only three diagonal entries are non-zero. The first principal axis is chosen to be along the axial shaft of gyroscope. The

second principal axis is chosen to be along the axis about which the gyroscope is tilting with angle α . The third principal axis chosen by applying right-hand rule to the previous axis. Denoting the first principal axis as ϕ -axis, the second principal axis as α -axis and the third principal axis as ξ -axis. Inertial tensor for the gyroscope can then be written as

$$I_{1,cm} = \begin{pmatrix} I_{\phi\phi} & 0 & 0 \\ 0 & I_{\xi\xi} & 0 \\ 0 & 0 & I_{\alpha\alpha} \end{pmatrix} \quad (3.8)$$

ϕ and α both are about their respective axes but θ is about the global y -axis thus we need to transform θ along the principal axes. Also, as gyroscope is first tilted by angle θ about y -axis and then by angle α about α -axis. Then total rotation matrix is the product of two rotation matrices. $\dot{\theta}$ in $\phi\alpha\xi$ -coordinate is given as

$$\omega'_{1,\theta} = \begin{pmatrix} \cos \alpha & \sin \alpha & 0 \\ -\sin \alpha & \cos \alpha & 0 \\ 0 & 0 & 1 \end{pmatrix} \begin{pmatrix} \cos \theta & 0 & -\sin \theta \\ 0 & 1 & 0 \\ \sin \theta & 0 & \cos \theta \end{pmatrix} \begin{pmatrix} 0 \\ \dot{\theta} \\ 0 \end{pmatrix} = \begin{pmatrix} \dot{\theta} \sin \alpha \\ \dot{\theta} \cos \alpha \\ 0 \end{pmatrix} \quad (3.9)$$

Angular velocity of the gyroscope can be found by adding $\omega'_{1,\theta}$ with contribution from ϕ and α . Thus, angular velocity of gyroscope is given as

$$\omega_1 = \omega'_{1,\theta} + \omega_{1,\phi} + \omega_{1,\alpha} \quad (3.10)$$

Substituting the values of $\omega'_{1,\theta}$, $\omega_{1,\phi}$ and $\omega_{1,\alpha}$ in above equation yields

$$\omega_1 = \begin{pmatrix} \dot{\theta} \sin \alpha \\ \dot{\theta} \cos \alpha \\ 0 \end{pmatrix} + \begin{pmatrix} \dot{\phi} \\ 0 \\ 0 \end{pmatrix} + \begin{pmatrix} 0 \\ 0 \\ \dot{\alpha} \end{pmatrix} = \begin{pmatrix} \dot{\phi} + \dot{\theta} \sin \alpha \\ \dot{\theta} \cos \alpha \\ \dot{\alpha} \end{pmatrix} \quad (3.11)$$

Thus, the kinetic energy of the gyroscope about its center of mass is given as

$$T_{g,1_{cm}} = \frac{1}{2} \omega_1^T I_{1,cm} \omega_1 \quad (3.12)$$

Substituting the values of ω_1 and $I_{1,cm}$ in the above equation yields

$$T_{g,1_{cm}} = \frac{1}{2} \begin{pmatrix} \dot{\phi} + \dot{\theta} \sin \alpha & \dot{\theta} \cos \alpha & \dot{\alpha} \end{pmatrix} \begin{pmatrix} I_{\phi\phi} & 0 & 0 \\ 0 & I_{\xi\xi} & 0 \\ 0 & 0 & I_{\alpha\alpha} \end{pmatrix} \begin{pmatrix} \dot{\phi} + \dot{\theta} \sin \alpha \\ \dot{\theta} \cos \alpha \\ \dot{\alpha} \end{pmatrix} \quad (3.12)$$

Matrix multiplication of above equation yields

$$T_{g,1_{cm}} = \frac{1}{2} I_{\phi\phi} (\dot{\phi} + \dot{\theta} \sin \alpha)^2 + \frac{1}{2} I_{\xi\xi} (\dot{\theta} \cos \alpha)^2 + \frac{1}{2} I_{\alpha\alpha} \dot{\alpha}^2 \quad (3.13)$$

Here $T_{g,1_{cm}}$ is the kinetic energy of the gyroscope about its center of mass.

The term $\frac{1}{2} m_{g,1} v_{g,1_{cm}}^2$ is the kinetic energy of the center of mass of the gyroscope. To determine the kinetic energy of the center of mass we need to determine $\mathbf{v}_{g,1_{cm}}$. The position of the center of mass of the first gyroscope from the origin is

$$\mathbf{r}_{g,1_{cm}} = (r_1 + l_1 \cos \alpha) \sin \theta \hat{i} + l_1 \sin \alpha \hat{j} + (r_1 + l_1 \cos \alpha) \cos \theta \hat{k} \quad (3.14)$$

differentiating the above equation yields

$$\begin{aligned} \mathbf{v}_{g,1_{cm}} = & ((r_1 + l_1 \cos \alpha) \cos \theta \dot{\theta} - l_1 \sin \alpha \sin \theta \dot{\alpha}) \hat{i} + l_1 \cos \alpha \dot{\alpha} \hat{j} \\ & + (- (r_1 + l_1 \cos \alpha) \sin \theta \dot{\theta} - l_1 \sin \alpha \cos \theta \dot{\alpha}) \hat{k} \end{aligned} \quad (3.15)$$

which is used to obtain the square of speed of the center of mass of gyroscope $v_{g,1_{cm}}^2$:

$$v_{g,1_{cm}}^2 = \mathbf{v}_{g,1_{cm}} \cdot \mathbf{v}_{g,1_{cm}} = \dot{\alpha}^2 l_1^2 + \dot{\theta}^2 (r_1 + l_1 \cos \alpha)^2 \quad (3.16)$$

We are now in the position to express total kinetic energy of the first gyroscope in terms of its parameters and components of the angular velocity. Total kinetic energy for the first gyroscope is

$$\begin{aligned} T_{g,1} = & \frac{1}{2} I_{\phi\phi} (\dot{\phi} + \dot{\theta} \sin \alpha)^2 + \frac{1}{2} I_{\xi\xi} (\dot{\theta} \cos \alpha)^2 + \frac{1}{2} I_{\alpha\alpha} \dot{\alpha}^2 \\ & + \frac{1}{2} m_{g,1} (\dot{\alpha}^2 l_1^2 + \dot{\theta}^2 (r_1 + l_1 \cos \alpha)^2) \end{aligned} \quad (3.17)$$

A similar expression of kinetic energy can be obtained for the second gyroscope, which is

$$T_{g,2} = \frac{1}{2} I_{\psi\psi} (\dot{\psi} + \dot{\theta} \sin \beta)^2 + \frac{1}{2} I_{\zeta\zeta} (\dot{\theta} \cos \beta)^2 + \frac{1}{2} I_{\beta\beta} \dot{\beta}^2 + \frac{1}{2} m_{g,2} (\dot{\beta}^2 l_2^2 + \dot{\theta}^2 (r_2 + l_2 \cos \beta)^2) \quad (3.18)$$

The kinetic energy of the motorbike itself is given as

$$T_b = \frac{1}{2} I_b \dot{\theta}^2 \quad (3.19)$$

here I_b is the moment of inertia of the motorbike with respect to ground about global y -axis. The total kinetic energy of the system can be obtained by summing up kinetic energies of the motorbike and the two gyroscopes:

$$T = T_b + T_{g,1} + T_{g,2} \quad (3.20)$$

Substituting values of T_b , $T_{g,1}$ and $T_{g,2}$ in the above equation yields

$$T = \frac{1}{2} I_b \dot{\theta}^2 + \frac{1}{2} I_{\phi\phi} (\dot{\phi} + \dot{\theta} \sin \alpha)^2 + \frac{1}{2} I_{\xi\xi} (\dot{\theta} \cos \alpha)^2 + \frac{1}{2} I_{\alpha\alpha} \dot{\alpha}^2 + \frac{1}{2} I_{\zeta\zeta} (\dot{\theta} \cos \beta)^2 + \frac{1}{2} m_{g,1} (\dot{\alpha}^2 l_1^2 + \dot{\theta}^2 (r_1 + l_1 \cos \alpha)^2) + \frac{1}{2} I_{\psi\psi} (\dot{\psi} + \dot{\theta} \sin \beta)^2 + \frac{1}{2} I_{\beta\beta} \dot{\beta}^2 + \frac{1}{2} m_{g,2} (\dot{\beta}^2 l_2^2 + \dot{\theta}^2 (r_2 + l_2 \cos \beta)^2) \quad (3.21)$$

Lagrangian of the system is defined as [14]

$$L = T - V \quad (3.22)$$

Substituting values of T and V in the above equation yields

$$L = \frac{1}{2} I_b \dot{\theta}^2 + \frac{1}{2} I_{\phi\phi} (\dot{\phi} + \dot{\theta} \sin \alpha)^2 + \frac{1}{2} I_{\xi\xi} (\dot{\theta} \cos \alpha)^2 + \frac{1}{2} I_{\alpha\alpha} \dot{\alpha}^2 - m_b g H \cos \theta + \frac{1}{2} m_{g,1} (\dot{\alpha}^2 l_1^2 + \dot{\theta}^2 (r_1 + l_1 \cos \alpha)^2) + \frac{1}{2} I_{\psi\psi} (\dot{\psi} + \dot{\theta} \sin \beta)^2 - m_{g,1} g (r_1 + l_1 \cos \alpha) \cos \theta - m_{g,2} g (r_2 + l_2 \cos \beta) \cos \theta \quad (3.23)$$

As ϕ and ψ are cyclic coordinates thus Routh's procedure can be employed to simplify finding the equations of motion of the system. The conjugate momentum for ϕ is

$$p_\phi = I_{\phi\phi}(\dot{\phi} + \dot{\theta} \sin \alpha) \quad (3.24)$$

And similarly, the conjugate momentum for ψ is

$$p_\psi = I_{\psi\psi}(\dot{\psi} + \dot{\theta} \sin \beta) \quad (3.25)$$

Using Legendre transformation to change variable from ϕ and ψ to p_ϕ and p_ψ for the Lagrangian. Routhian for the system is defined as

$$R = \dot{\phi} p_\phi + \dot{\psi} p_\psi - L \quad (3.26)$$

Solving equation 3.24 and 3.25 for ϕ and ψ respectively and replacing in above equation to obtain

$$\begin{aligned} R = & -p_\phi \dot{\theta} \sin \alpha - p_\psi \dot{\theta} \sin \beta - \frac{1}{2} I_b \dot{\theta}^2 + \frac{1}{2} \frac{p_\phi^2}{I_{\phi\phi}} - \frac{1}{2} I_{\xi\xi} (\dot{\theta} \cos \alpha)^2 - \frac{1}{2} I_{\alpha\alpha} \dot{\alpha}^2 - \frac{1}{2} m_{g,1} (\dot{\alpha}^2 l_1^2 + \dot{\theta}^2 (r_1 + l_1 \cos \alpha)^2) + \frac{1}{2} \frac{p_\psi^2}{I_{\psi\psi}} \\ & + m_{g,1} g (r_1 + l_1 \cos \alpha) \cos \theta + m_{g,2} g (r_2 + l_2 \cos \beta) \cos \theta \end{aligned} \quad (3.27)$$

The Routhian acts as Lagrangian in untransformed coordinates and Hamiltonian in transformed coordinates. Equation of motion in θ can be found as

$$\frac{d}{dt} \left(\frac{\partial R}{\partial \dot{\theta}} \right) - \frac{\partial R}{\partial \theta} = 0 \quad (3.28)$$

Similarly, equations of motion in α and β can be found as

$$\frac{d}{dt} \left(\frac{\partial R}{\partial \dot{\alpha}} \right) - \frac{\partial R}{\partial \alpha} = T_\alpha \quad (3.29)$$

$$\frac{d}{dt} \left(\frac{\partial R}{\partial \dot{\beta}} \right) - \frac{\partial R}{\partial \beta} = T_\beta \quad (3.30)$$

where T_α and T_β are torque on the first and second gyroscopes, respectively.
The equations of motion in φ and ψ are

$$\dot{\phi} = \frac{\partial R}{\partial p_\phi} \quad (3.31)$$

$$\dot{p}_\phi = 0 \quad (3.31)$$

$$\dot{\psi} = \frac{\partial R}{\partial p_\psi} \quad (3.32)$$

$$\dot{p}_\psi = 0 \quad (3.33)$$

After substituting the value of Routhian in the above equations and simplifying, the equation of motion in theta is:

$$\begin{aligned} & \left(I_b + m_{g,1}(r_1 + l_1 \cos \alpha)^2 + m_{g,2}(r_2 + l_2 \cos \beta)^2 + I_{\xi\xi} \cos^2 \alpha + I_{\zeta\zeta} \cos^2 \beta \right) \ddot{\theta} - 2 \left(I_{\xi\xi} \cos \alpha \sin \alpha \dot{\alpha} + I_{\zeta\zeta} \cos \beta \sin \beta \dot{\beta} + m_g \right. \\ & \left. \textcolor{red}{\cancel{m_b g H}} + m_{g,1} g (r_1 + l_1 \cos \alpha) + m_{g,2} g (r_2 + l_2 \cos \beta) \right) \sin \theta \end{aligned} \quad (3.34)$$

the equation of motion in α is:

$$\begin{aligned} & \left(I_{\alpha\alpha} + m_{g,1} l_1^2 \right) \ddot{\alpha} = T_\alpha - m_{g,1} (r_1 + l_1 \cos \alpha) l_1 \sin \alpha \dot{\theta}^2 + p_\phi \dot{\theta} \cos \alpha \\ & - I_{\xi\xi} \cos \alpha \sin \alpha \dot{\theta}^2 + m_{g,1} g l_1 \sin \alpha \cos \theta \end{aligned} \quad (3.35)$$

the equation of motion in β is:

$$\begin{aligned} & \left(I_{\beta\beta} + m_{g,2} l_2^2 \right) \ddot{\beta} = T_\beta - m_{g,2} (r_2 + l_2 \cos \beta) l_2 \sin \beta \dot{\theta}^2 + p_\psi \dot{\theta} \cos \beta \\ & - I_{\zeta\zeta} \cos \beta \sin \beta \dot{\theta}^2 + m_{g,2} g l_2 \sin \beta \cos \theta \end{aligned} \quad (3.36)$$

the equations of motion in φ is:

$$\dot{\phi} = \frac{p_\phi}{I_{\phi\phi}} - \dot{\theta} \sin \alpha \quad (3.37)$$

$$(\dot{\phi} + \dot{\theta} \sin \alpha)_i = (\dot{\phi} + \dot{\theta} \sin \alpha)_f \quad (3.38)$$

the equations of motion in ψ is:

$$\dot{\psi} = \frac{p_\psi}{I_{\psi\psi}} - \dot{\theta} \sin \beta (\dot{\psi} + \dot{\theta} \sin \beta)_i = (\dot{\psi} + \dot{\theta} \sin \beta)_f \quad (3.40)$$

Equation 3.38 and 3.40 are obtained by solving equation 3.31 and 3.33 respectively and they simply represent the statement of conservation of conjugate momentum in ϕ and ψ . Solution of equations 3.37 and 3.39 are unnecessary as they give ϕ and ψ as a function of time, thus detail of these coordinates is unnecessary. Though variations in ϕ and ψ are important to determine in understanding of the system.

If the motion of gyroscopes is being controlled by the motors and there are no other forces acting, then T_α and T_β are given by:

$$T_\alpha = K_{T,1} i_1 \quad (3.41)$$

$$T_\beta = K_{T,2} i_2 \quad (3.42)$$

where $K_{T,1}$ and $K_{T,2}$ are motor torque constants of first and second motor respectively and i_1 and i_2 are currents passing through the first and second motor, respectively. L_1 , R_1 and $K_{b,1}$ are the inductance, resistance and back emf constant of the electric circuit of first motor respectively and V_1 is the voltage applied across the first circuit. In a similar manner, L_2 , R_2 , $K_{b,2}$ and V_2 are defined for the electric circuit of the second motor. Thus, motor circuit equations from Kirchhoff's Voltage law are:

$$L_1 \frac{di_1}{dt} + R_1 i_1 + K_{b,1} \dot{\alpha} = V_1 \quad (3.43)$$

$$L_2 \frac{di_2}{dt} + R_2 i_2 + K_{b,2} \dot{\beta} = V_2 \quad (3.44)$$

The conjugate momentum in α and β for the system are obtained as

$$p_\alpha = \frac{\partial L}{\partial \dot{\alpha}} = (I_{\alpha\alpha} + m_{g,1} l_1^2) \dot{\alpha} \quad (3.45)$$

$$p_\beta = \frac{\partial L}{\partial \dot{\beta}} = (I_{\beta\beta} + m_{g,2}l_2^2)\dot{\beta} \quad (3.46)$$

and the conjugate momentum in θ for the system is obtained as

$$\begin{aligned} p_\theta = \frac{\partial L}{\partial \dot{\theta}} &= I_b \dot{\theta} + I_{\phi\phi} (\dot{\phi} + \dot{\theta} \sin \alpha) \sin \alpha + I_{\xi\xi} (\cos \alpha)^2 \dot{\theta} + m_{g,1} (r_1 + l_1 \cos \alpha)^2 \dot{\theta} \\ &+ I_{\psi\psi} (\dot{\psi} + \dot{\theta} \sin \beta) \sin \beta + I_{\zeta\zeta} (\cos \beta)^2 \dot{\theta} + m_{g,2} (r_2 + l_2 \cos \beta)^2 \dot{\theta} \end{aligned} \quad (3.47)$$

The energy equation for the system can be determined as

$$h = \dot{\theta} \frac{\partial L}{\partial \dot{\theta}} + \dot{\alpha} \frac{\partial L}{\partial \dot{\alpha}} + \dot{\beta} \frac{\partial L}{\partial \dot{\beta}} + \dot{\phi} \frac{\partial L}{\partial \dot{\phi}} + \dot{\psi} \frac{\partial L}{\partial \dot{\psi}} - L \quad (3.48)$$

The above equation can be simplified to obtain,

$$\begin{aligned} h &= \frac{1}{2} I_b \dot{\theta}^2 + \frac{1}{2} I_{\phi\phi} (\dot{\phi} + \dot{\theta} \sin \alpha)^2 + \frac{1}{2} I_{\xi\xi} (\dot{\theta} \cos \alpha)^2 + \frac{1}{2} I_{\alpha\alpha} \dot{\alpha}^2 + \frac{1}{2} I_{\zeta\zeta} (\dot{\theta} \cos \beta)^2 + \frac{1}{2} m_{g,1} (\dot{\alpha}^2 l_1^2 + \dot{\theta}^2 (r_1 + l_1 \cos \alpha)^2) + \frac{1}{2} I_{\psi\psi} \\ &+ m_{g,2} g (r_2 + l_2 \cos \beta) \cos \theta + m_b g H \cos \theta \end{aligned} \quad (3.49)$$

If we consider symmetrical gyroscopes, motors, and electric components along with the rotating and tilting motors in the opposite directions, this results in the simplification of equation of motions. Under the assumptions, $\phi = -\psi$, $\alpha = -\beta$, $I_{\alpha\alpha} = I_{\beta\beta}$, $I_{\xi\xi} = I_{\zeta\zeta}$, $I_{\phi\phi} = I_{\psi\psi}$, $m_{g,1} = m_{g,2} = mg$, $l_1 = l_2 = l$, $r_1 = r_2 = r$, $i_1 = -i_2$, $K_{T,1} = K_{T,2} = K_T$, $L_1 = L_2$, $R_1 = R_2$, $K_{b,1} = K_{b,2} = K_b$ and $V_1 = -V_2$ the equations of motion for θ is

$$\begin{aligned} &(I_b + 2m_g(r + l \cos \alpha)^2 + 2I_{\xi\xi} \cos^2 \alpha) \ddot{\theta} - 4(I_{\xi\xi} \cos \alpha \sin \alpha \dot{\alpha} + m_g(r + l \cos \alpha) l \sin \alpha \dot{\alpha}) \dot{\theta} \\ &+ 2p_\phi \cos \alpha \dot{\alpha} = (m_b g H + 2m_g g(r + l \cos \alpha)) \sin \theta \end{aligned} \quad (3.50)$$

The equation of motion for tilting (α and β) of both gyroscopes is

$$\begin{aligned} &(I_{\alpha\alpha} + m_g l^2) \ddot{\alpha} = T_\alpha - m_g(r + l \cos \alpha) l \sin \alpha \dot{\theta}^2 + p_\phi \dot{\theta} \cos \alpha \\ &- I_{\xi\xi} \cos \alpha \sin \alpha \dot{\theta}^2 + m_g g l \sin \alpha \cos \theta \end{aligned} \quad (3.51)$$

The equations of motion for spinning (ϕ and ψ) of both gyroscopes are

$$\dot{\phi} = \frac{p_\phi}{I_{\phi\phi}} - \dot{\theta} \sin \alpha \quad (3.52)$$

$$(\dot{\phi} + \dot{\theta} \sin \alpha)_i = (\dot{\phi} + \dot{\theta} \sin \alpha)_f \quad (3.53)$$

The torque acting on the gyroscopes due to motors is given as

$$T_\alpha = K_T i_1 \quad (3.54)$$

The equation of motion for both motor circuits is

$$L_1 \frac{di_1}{dt} + R_1 i_1 + K_b \dot{\alpha} = V_1 \quad (3.55)$$

3.2 Gyroscope Design

To design a suitable gyroscope, it is necessary to determine the moment of inertia. Consider a cylindrical disk with a cylindrical rod passing through it. Let ' R_1 ' be the radius of disk and ' L_1 ' be the thickness of the disk. Similarly, let R_2 be the radius of the rod and L_2 be the length of rod. The disk is placed at a height of h from the base of rod. Then the mass of gyroscope will be

$$m_g = \int_V \rho dV \quad (3.56)$$

$$m_g = \rho \pi (R_2^2 L_2 + (R_1^2 - R_2^2) L_1) \quad (3.57)$$

The z component of the center of mass of gyroscope is

$$z_{cm} = \frac{1}{m_g} \int_V \rho z dV \quad (3.58)$$

$$z_{cm} = \frac{\rho\pi}{m_g} \left(\frac{R_2^2 L_2^2}{2} + (R_1^2 - R_2^2) L_1 \left(h + \frac{L_1}{2} \right) \right) \quad (3.59)$$

The moment of inertia of gyroscope about α -axis evaluated at the base of the rod is

$$\begin{aligned} I_{\alpha\alpha, end} &= \int_0^h \int_0^{R_2} \rho\pi(r^2 + 2z^2) r dr dz + \int_h^{h+L_1} \int_0^{R_1} \rho\pi(r^2 + 2z^2) r dr dz \\ &\quad + \int_{h+L_1}^{L_2} \int_0^{R_2} \rho\pi(r^2 + 2z^2) r dr dz \end{aligned} \quad (3.60)$$

$$\begin{aligned} I_{\alpha\alpha, end} &= \rho\pi \left(\frac{hR_2^4}{4} + \frac{h^3 R_2^2}{3} + \frac{L_1 R_1^4}{4} + \frac{R_1^2}{3} ((h+L_1)^3 - h^3) + \frac{R_2^4}{4} (L_2 - L_1 - h) \right) \\ &\quad + \frac{\rho\pi R_2^2}{3} (L_2^3 - (h+L_1)^3) \end{aligned} \quad (3.61)$$

The moment of inertia about ξ -axis is equal to that of α -axis due to symmetry. Thus, the moment of inertia of gyroscope about both α and ξ axis at the center of mass can then be evaluated by using parallel-axis theorem.

$$I_{\xi\xi} = I_{\alpha\alpha} = I_{\alpha\alpha, end} - m_g z_{cm}^2 \quad (3.62)$$

The moment of inertia of gyroscope about ϕ -axis at center of mass can then be written as

$$I_{\phi\phi} = \frac{1}{2} \rho\pi (R_1^4 L_1 + R_2^4 (L_2 - L_1)) \quad (3.63)$$

3.2.1 Size Optimizations

Large value of $I_{\phi\phi}$ results in a large value of p_ϕ which in turn increases the stability by enlarging the restoring term $2p_\phi \cos\alpha \dot{\alpha}$. Thus, maximizing value of $I_{\phi\phi}$ is important. But increasing $I_{\phi\phi}$ increases the size of the gyroscope which is undesirable. To make the design compact, the distance to the furthest point on the gyroscope has to be minimized. To accomplish this, we are assuming that $R_2 \ll R_1$ and $L_2 < 2R_1$, 3.63 then reduces to

$$I_{\phi\phi} = \frac{1}{2} \rho \pi R_1^4 L_1$$

(3.64)

In such a case as $L_2 < 2R_1$ the furthest distance point in gyroscope is given as

$$l_{lar} = \sqrt{\left(R_1\right)^2 + \left(\frac{L_1}{2}\right)^2}$$

(3.65)

Thus, $I_{\phi\phi}$ needs to be maximized to provide more stability and l_{lar} needs to be minimized to make the design more compact. As this is an optimization in two variables, thus some compromise has to be made between the two. So, to solve the above problem in this scenario, equation 3.65 can be used to solve for L_1 in terms of l_{lar} and the result can be substituted in equation 3.64 to obtain

$$I_{\phi\phi} = \rho \pi R_1^4 \sqrt{l_{lar}^2 - R_1^2}$$

(3.66)

Now to maximize $I_{\phi\phi}$ with respect to R_1 , taking the derivative of equation 3.66 with respect to R_1 and setting it equal to zero

$$\frac{d I_{\phi\phi}}{d R_1} = \frac{d}{d R_1} \left(\rho \pi R_1^4 \sqrt{l_{lar}^2 - R_1^2} \right) = 0$$

(3.67)

Solving the above equation to obtain values of R_1 and L_1 in terms of l_{lar} .

$$R_1 = \sqrt{\frac{4}{5}} l_{lar}$$

(3.68)

$$L_1 = \sqrt{\frac{4}{5}} l_{lar}$$

(3.69)

To check it is a maximum, the second derivative of $I_{\phi\phi}$ at the above values of R_1 needs to be evaluated.

$$\frac{d^2 I_{\phi\phi}}{d R_1^2} = \frac{-1025}{125} \rho^2 \pi^2 l_{lar}^8$$

(3.70)

which is negative thus it is a maximum.

The problem with the above limitations is that it results in large mass near the axis of rotation, so a large mass is required which in turn increases the cost because of the larger material requirement. But otherwise, this results in a compact design.

3.3 Solutions of the Controlled System

The main purpose is to make the system achieve a final state of $\theta=0$, $\dot{\theta}=0$, $\alpha=0$ and $\dot{\alpha}=0$. This is so that the motorbike and both the gyroscopes are stationary and are aligned with the vertical. To obtain the solutions for the controlled system, it is first useful to remove some negligible terms along with some linearization and assumptions. Under the following assumptions

- $2mg(r+l\cos\alpha)^2 \approx 2mgr^2 + 4mgl$ as $r^2 \gg l^2 \cos^2 \alpha$ and $\cos\alpha \approx 1$.
- $I_b + 2mgr^2 + 4mgl \gg 2I_\xi \cos^2 \alpha$.
- $4(I_\xi \cos\alpha \sin\alpha \dot{\alpha} + mg(r+l\cos\alpha)l \sin\alpha \dot{\alpha}) \theta \ll (mbgH + 2m_g g(r+l)) \sin\theta - 2p_\phi \cos\alpha \dot{\alpha}$
- $2m_g g(r+l\cos\alpha) \approx 2m_g g(r+l)$.
- $m_g(r+l\cos\alpha)l \sin\alpha \dot{\theta}^2 + I_\xi \cos\alpha \sin\alpha \dot{\theta}^2 \ll p_\phi \dot{\theta} \cos\alpha + m_g g l \sin\alpha \cos\theta$.
- $\cos\theta \approx 1$.

the equations 3.50 and 3.51 reduce to

$$(I_b + 2m_g r^2 + 4m_g rl) \ddot{\theta} + 2p_\phi \cos\alpha \dot{\alpha} = (m_b g H + 2m_g g(r+l)) \sin\theta$$

(3.71)

$$(I_{\alpha\alpha} + m_g l^2) \ddot{\alpha} = T + p_\phi \dot{\theta} \cos\alpha + m_g g l \sin\alpha \cos\theta$$

(3.72)

Consider the following substitution

$$\dot{\alpha} \cos \alpha = k_1 \sin \theta + k_2 \dot{\theta} + k_3 \alpha \quad (3.73)$$

where k_1 , k_2 and k_3 constants. The above substitution along with approximation $\sin \theta \approx \theta$ reduces equation 3.71 to

$$(I_b + 2m_g r^2 + 4m_g rl) \ddot{\theta} + 2p_\phi k_2 \dot{\theta} + (2p_\phi k_1 - (m_b gH + 2m_g g(r+l)))\theta \dot{i} - 2p_\phi k_3 \quad (3.74)$$

which is a familiar equation of forced-damped vibratory system if $2p_\phi k_1 - (m_b gR + 2m_g g(r+l)) > 0$. Thus,

$$k_1 > \frac{(m_b gH + 2m_g g(r+l))}{2p_\phi} \quad (3.75)$$

And if the system is critically damped the critical value of k_2 will be

$$k_{2,c} = \frac{2\sqrt{(2p_\phi k_1 - (m_b gH + 2m_g g(r+l)))(I_b + 2m_g r^2 + 4m_g rl)}}{2p_\phi} \quad (3.76)$$

For overdamped, k_2 will be larger than $k_{2,c}$ and in an underdamped scenario, k_2 will be smaller than $k_{2,c}$.

$$k_2 < k_{2,c} \text{ for underdamped system}$$

$$k_2 > k_{2,c} \text{ for overdamped system}$$

Only existence of term $k_1 \sin \theta + k_2 \dot{\theta}$ results in a non-zero final value for α so $k_3 \alpha$ term is added to ensure zero final value for α . To obtain the solution of the system, equation 3.41 and 3.43 with $\cos \alpha \approx 1$ is used to avoid the division by a small number for large values of α . Due to approximation, equation 3.73 reduces to the following equation.

$$\dot{\alpha} = k_1 \sin \theta + k_2 \dot{\theta} + k_3 \alpha \quad (3.77)$$

which are then solved simultaneously using runge-kutta method of order 4 [16]. The equation 3.51 is then used to solve for required torque applied to the gyroscopes.

Equations 3.54 and 3.55 are then used to solve for current and required voltage, respectively.

3.3.1 Plots

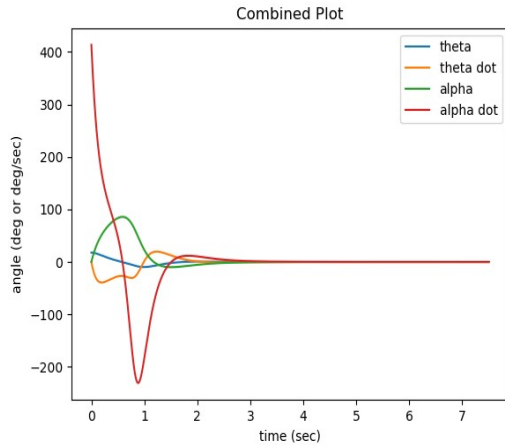


Figure 9: Combined Plot

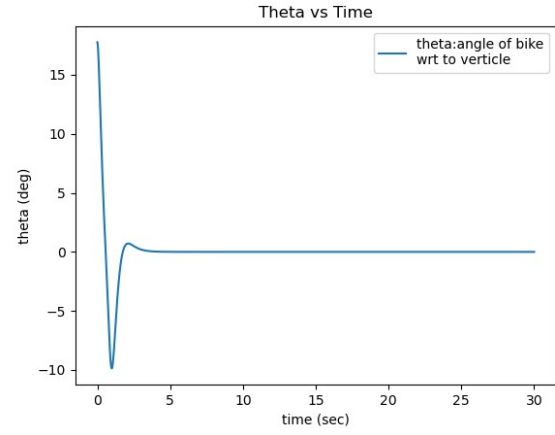


Figure 10: Theta vs Time

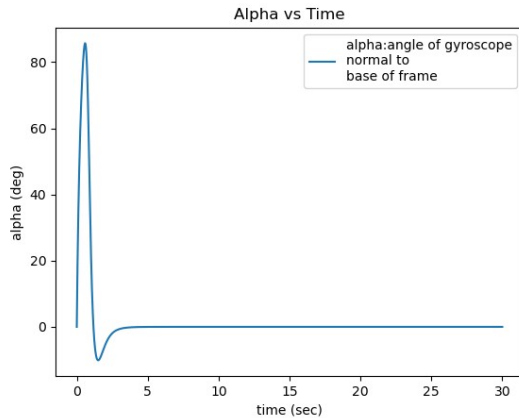


Figure 11: Alpha vs Time

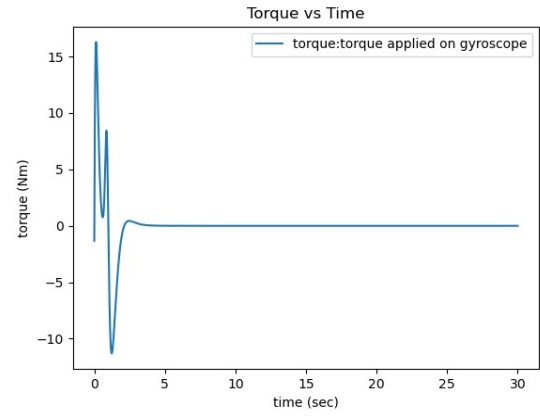


Figure 12: Torque vs Time

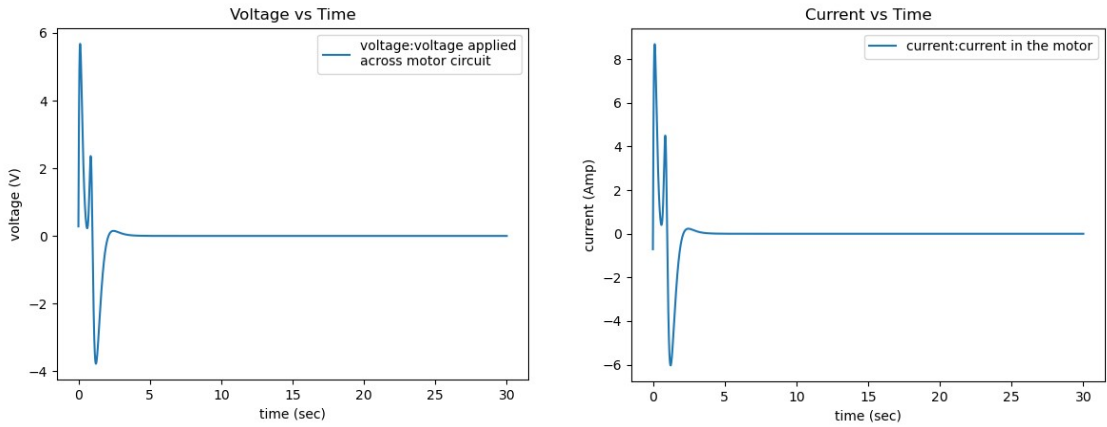


Figure 13: Voltage vs Time

Figure 14: Current vs Time

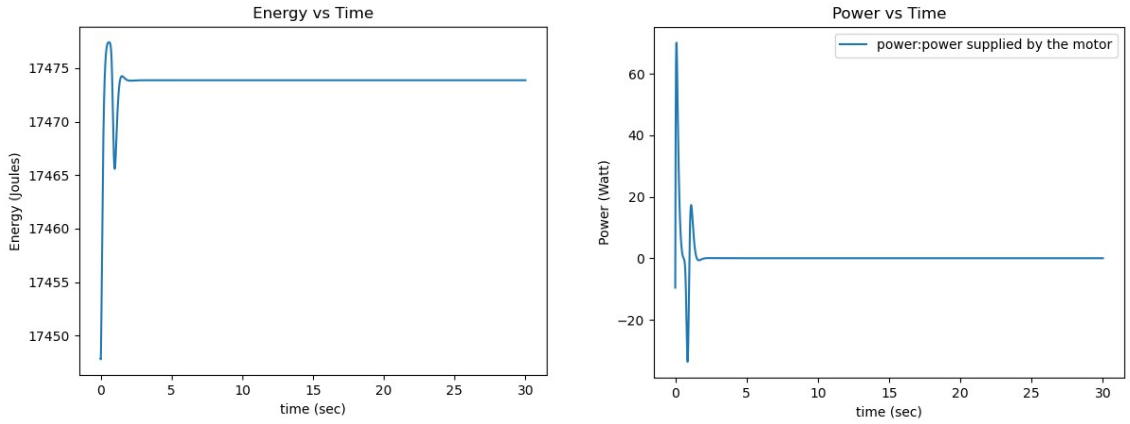


Figure 15: Energy vs Time

Figure 16: Power vs Time

3.3.2 Discussion

Certain important parameters for the motion of the motorbike-gyroscope system are plotted against time. Figure 10 is the plot of theta, which is the angle of the motorbike from vertical (Roll angle) vs time. The gyroscopes can recover the motorbike from a 17° angle tilt. The variation in the tilt angle of the gyroscopes with time is shown by Figure 11. The gyroscopes tilt to about 80° . Figure 9 shows the plot of θ , $\dot{\theta}$, α and $\dot{\alpha}$ with respect to time. Variation of torque acting on the gyroscopes about tilt axis is given by Figure 12, the maximum value is about 20 Nm . Figure 13 shows the variation of voltage applied across the ends of circuit attached to the motor that exerts torque on the gyroscope. Figure 14 shows the current flowing through the circuit of the motor. Maximum voltage applied across circuit is 6 V and the maximum current flowing through the circuit is 10 A . Final energy state of the system is higher than

that of the initial state as the center of mass of the system is raised in the gravitational field which is indicated in the Figure 15. Power supplied by the motors to the gyroscopes reaches a maximum of 100 W and reaches steady value of zero as system achieves stable state as indicated by Figure 16.

3.4 Self-Balancing Action of the Control Moment Gyroscope System:

Summarizing the equations of the dynamic model of the motorcycle, the following equations are obtained,

$$(I_b + 2m_g r^2 + 4m_g rl)\ddot{\theta} + p_\phi \dot{\alpha} = (m_b gH + 2m_g g(r+l))\theta \quad (3.78)$$

$$Input = V = K_e \dot{\alpha} + Ri + L \frac{di}{dt} \quad (3.79)$$

$$Output = \ddot{\alpha} = \frac{K_T i + p_\phi \dot{\theta} + m_g g \alpha}{(I_{aa} + m_g l^2)} \quad (3.80)$$

Using these above mentioned equations, following definitions are made: $x = \begin{bmatrix} \theta \\ \dot{\theta} \\ \alpha \\ \dot{\alpha} \\ i \end{bmatrix}$, $y = \theta$,

and $u = U$. The mathematical model for the dynamics of the system in state space representation would then be as following:

$$\dot{x} = Ax + Bu$$

$$y = Cx + Du$$

Where A, B, C & D are defined as follows,

$$A = \begin{bmatrix} 0 & 1 & 0 & 0 & 0 \\ \frac{m_b g H + 2 m_g g (r+l)}{I_b + 2 m_g r^2 + 4 m_g r l} & 0 & 0 & \frac{P_\varphi}{I_b + 2 m_g r^2 + 4 m_g r l} & 0 \\ 0 & 0 & 0 & 1 & 0 \\ 0 & \frac{-P_\varphi}{2 I_{\alpha\alpha} + 2 m_g l^2} & \frac{m_g g l}{I_{\alpha\alpha} + m_g l^2} & 0 & \frac{K_t}{I_{\alpha\alpha} + m_g l^2} \\ 0 & 0 & 0 & \frac{-K_e}{L} & \frac{-R}{L} \end{bmatrix}$$

$$B = \begin{bmatrix} 0 \\ 0 \\ 0 \\ 0 \\ \frac{1}{L} \end{bmatrix}, C = [1 \ 0 \ 0 \ 0 \ 0], D = 0$$

A Control Moment Gyroscope has been designed for the motorbike model with the parameters as listed in Table 1. One of the most popular motorcycles that are used in Pakistan is being used for the scope of this project i.e., Honda CG125, which has a cumulative mass of approximately 180kg with a rider onboard. The dimensions of the two rotating masses (flywheels) were designed as to generate the required balancing torque. A hub motor was used to rotate the flywheel to a rather high angular speed of 4775 revolutions per minute. This will ensure a maximum balancing torque when the flywheels are tilted about their axes.

Table 1: Parameters and their Values

Parameters	Value	Unit	Description
m_g	6.2155	kg	Mass of gyroscope
m_b	180	kg	Mass of motorbike
r	0.45	m	Pivot Point of gyro from ground
l	0	m	COG of gyro from pivot point
H	0.3	m	Motorbike COG upright height
I_b	30	kg.m ²	Motorbike MOI around ground contact line
$I_{\varphi\varphi}$	0.067557	kg.m ²	Flywheel polar MOI around COG

I_{aa}	0.035095	kg.m ²	Flywheel radial MOI around COG
ω	500	rad/s	Flywheel angular velocity
L	0.000119	H	Motor Inductance
R	0.61	Ω	Motor Resistance
P_ϕ	67.557	kg.m ² /s	$P_\phi = 2 I_{\phi\phi} \dot{\theta}$
K_t	1.875	Nm/A	Motor torque constant
K_e	0.096	V.s	Motor back emf constant

Using the values of the parameters from the table above, the values for the state space matrices can be calculated as follows:

$$A = \begin{bmatrix} 0 & 1 & 0 & 0 & 0 \\ 18 & 0 & 0 & 2.1 & 0 \\ 0 & 0 & 0 & 1 & 0 \\ 0 & -962.5 & 0 & 0 & 53.4 \\ 0 & 0 & 0 & -806.7 & -5126.1 \end{bmatrix}$$

$$B = \begin{bmatrix} 0 \\ 0 \\ 0 \\ 0 \\ 8403.4 \end{bmatrix}, C = [1 \ 0 \ 0 \ 0 \ 0], D = 0$$

Using MATLAB to convert this state space matrix into a transfer function, the following transfer function is derived:

$$\frac{\theta(s)}{V(s)} = \frac{(9.328 \times 10^5)s}{s^5 + 5126s^4 + (4.508 \times 10^4)s^3 + (1.016 \times 10^7)s^2 - (7.741 \times 10^5)s} \quad (3.81)$$

This transfer function denotes the behaviour of the uncontrolled dynamic system of the attached gyroscope on the motorcycle. Since this system is uncompensated for, first its stability using control systems methods has to be analysed.

3.4.1 Stability Analysis of the Uncontrolled System:

MATLAB was used as the software platform to check for the stability of the uncontrolled dynamic system. The dynamic model was created on the platform and by using various commands and tools such as Pole Zero Plots, Step Response, Bode Plots etc., system stability can be analyzed, and these calculations can then even be used to design a control system for the derived dynamic model. [19]

Using the designed model on MATLAB, a pole-zero analysis on the uncontrolled system was conducted and the results are indicative that there are five poles and one zero for the uncontrolled system. Of these five poles, one is located on the right hand plane as can be observed from Figure 18 below. This is indicative of the fact that the uncontrolled and uncompensated-for system is innately unstable.

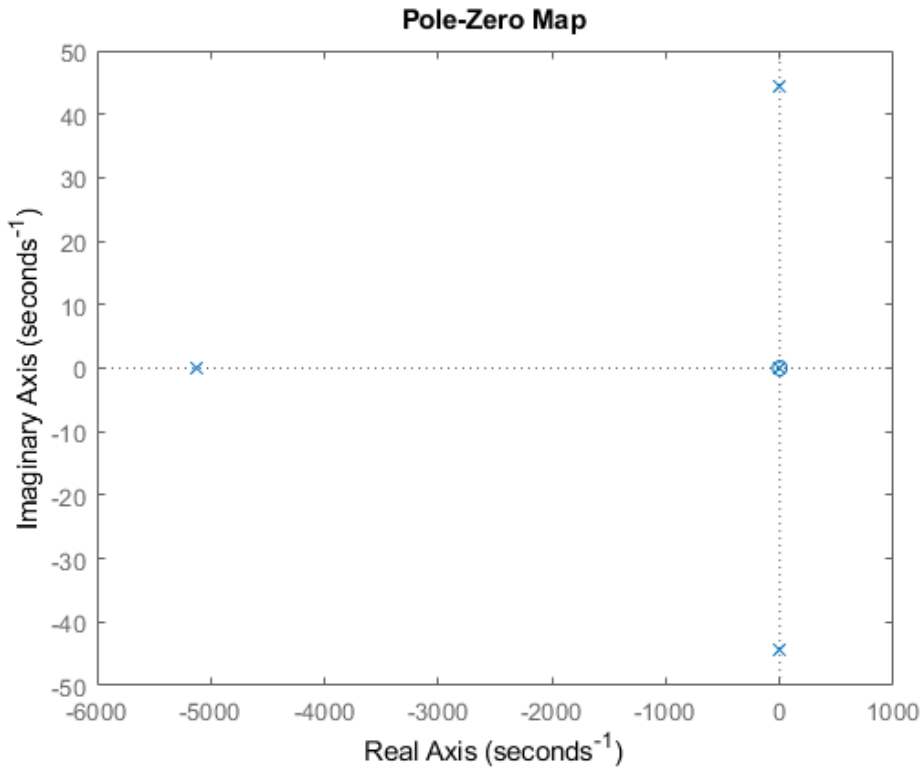


Figure 17: Pole Zero Plot

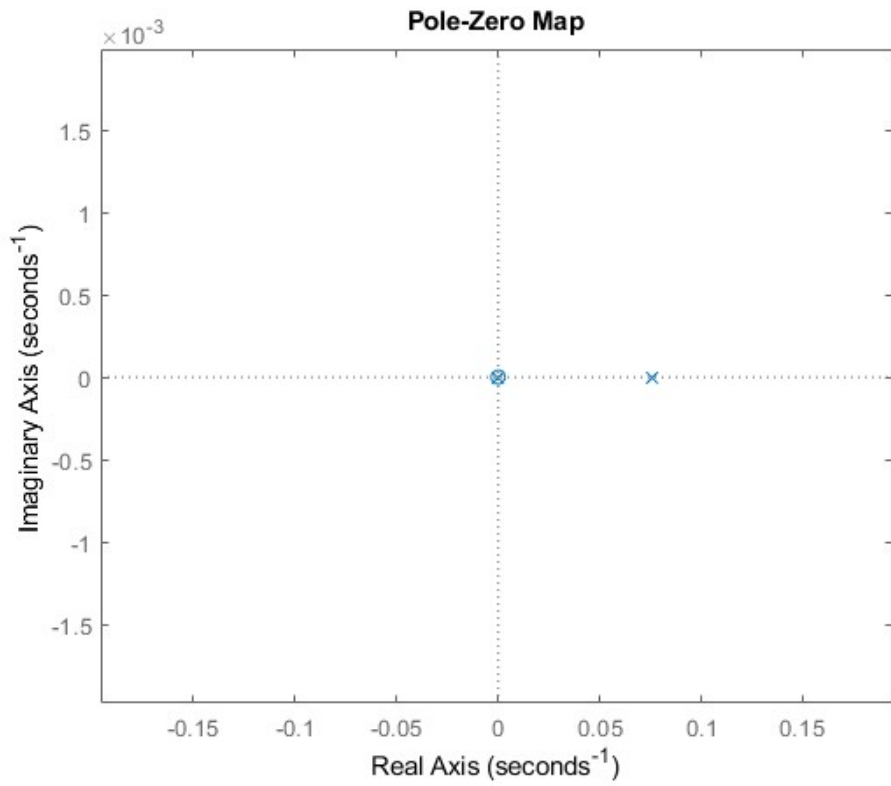


Figure 18: Pole Zero Plot (Zoomed)

To further verify the observed results and analyze the stability further, bode plot and step response were done on MATLAB interface as shown by Figure 19, Figure 20 and are indicative that the dynamic model is innately unstable. The bode plot, however, shows positive phase and gain margins of 33.9deg @ 0.0511rad/s and 39.3dB @ 44.5rad/s respectively, which indicate stability, but the step response further verifies that the amplitude approaches infinity with the passage of time, hence, proving the instability.

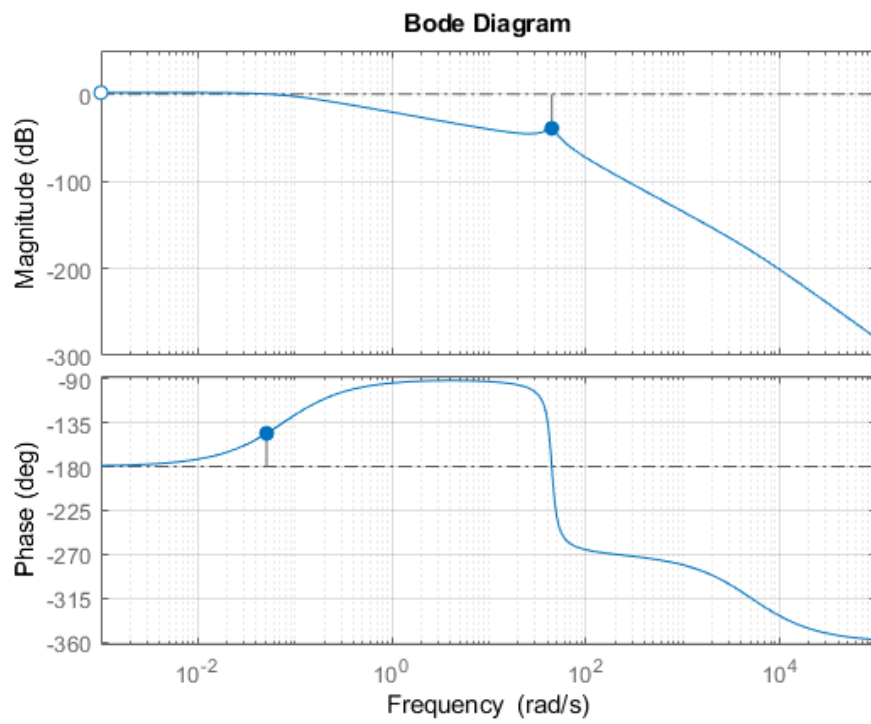


Figure 19: Bode Plot

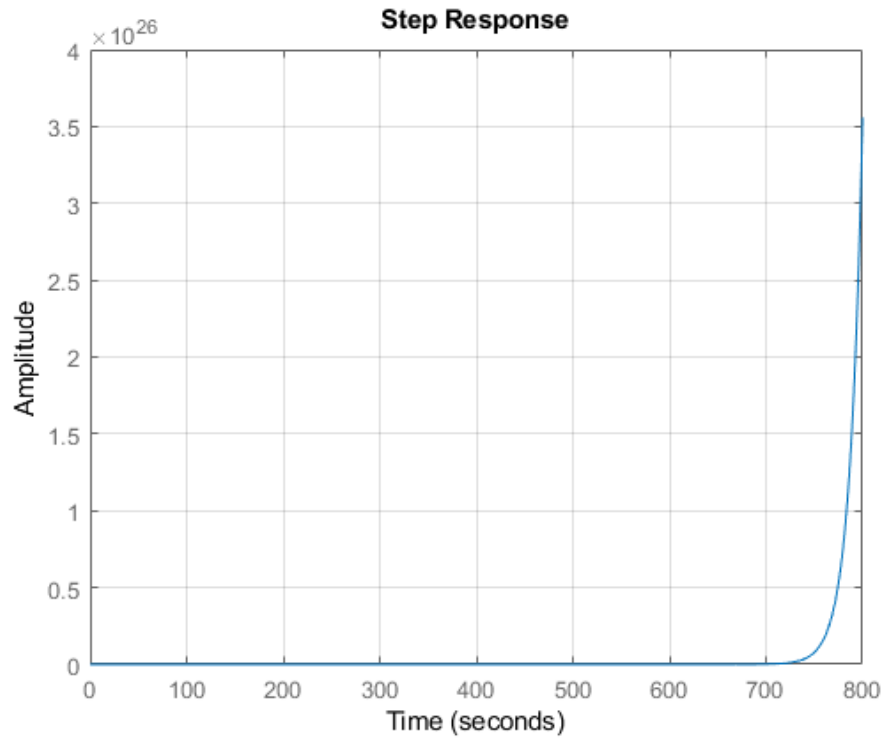


Figure 20: Step Response

3.4.2 Analysis of Proportional Integral Derivative (PID) Controlled System:

As it has been proven above that the system on its own is unstable, hence, a controller has to be designed for this system as to help the two-wheeler motorbike to always remained balanced. For this purpose, a PID Controller was implemented in SimuLink and tuned in order to set its gains. Simulink is equipped with a PID Tuner that helped set the gains for our controller so that it effectively balances the motorcycle and maintain its steady state position. The initial values of the gains to be put in the tuner were calculated using Zeigler-Nichols rules for tuning [20].

A block diagram was created in SimuLink as shown in Figure 21 entailing a controller applied to the un-controlled transfer function obtained from the dynamic model of the system.

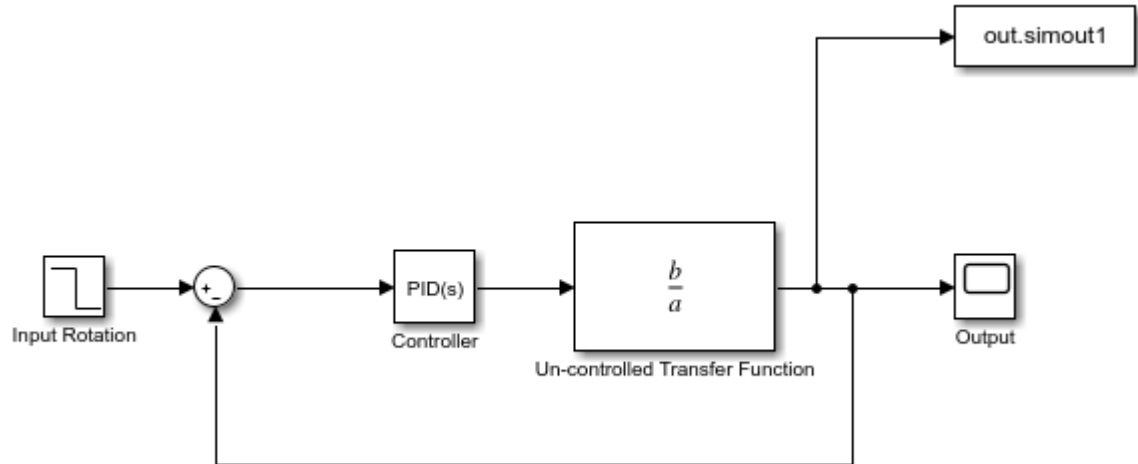


Figure 21: Control System Block Diagram

The gains were tuned to be as follows: $K_p = 34.4$, $K_i = 21.6$, $K_d = 3.0$ and $K_n = 3.7$. The exact values of the gains calculated by MATLAB SimuLink are mentioned in . The respective characteristics for the designed controller of our system are shown in Figure 22, Table 2 and Table 3 below. A **rise time of 0.453 seconds**, **settling time of 4.18 seconds**, and an **overshoot percentage of 11.7%** was observed which are all decent performance indicators for the project. Phase Margin and Gain Margin are also seen to be positive for the system which are indicative of the system's stability and can be seen as such in the bode plot plotted in Figure 23.

Further performance indicators are also plotted including Input Disturbance Rejection (Figure 24), Output Disturbance Rejection (Figure 25) and Controller Effort (Figure 26) all as a function of time. All these indicate a very decent performance of the designed controller with realistic values.

At the end to prove for the stability of the system, a pole zero map was also plotted as shown in Figure 27 and Figure 28. As can be observed there are no poles on the right hand plane for the controlled system, this exhibits the stability of the system after successful application of the PID controller.

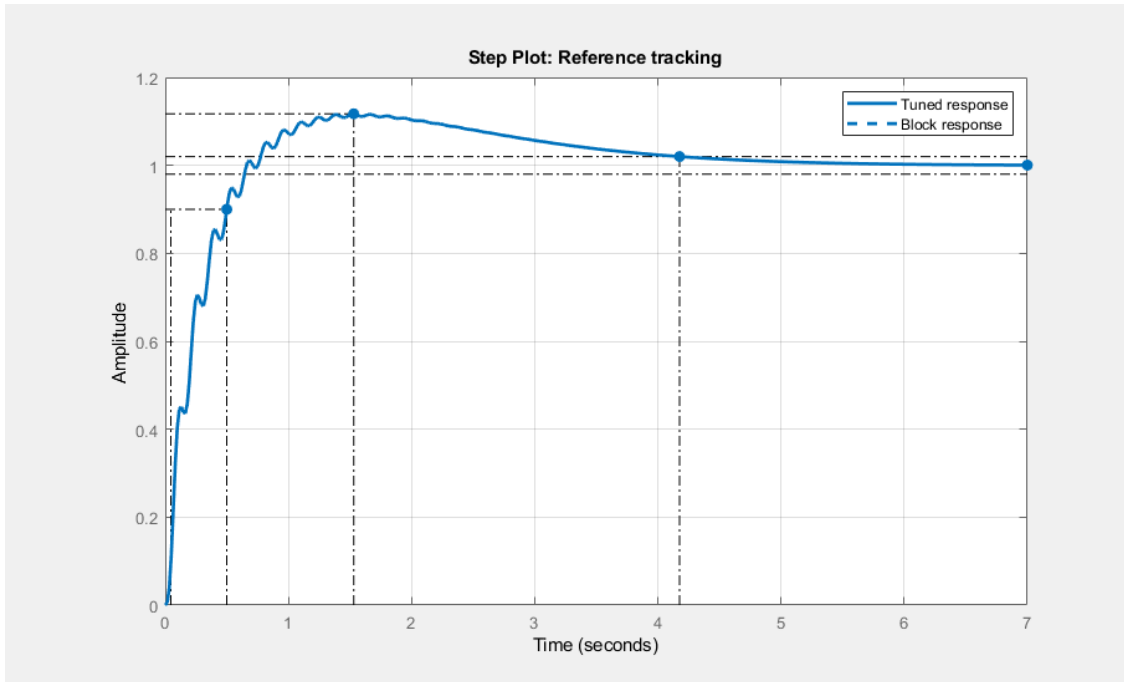


Figure 22: Step Plot - Reference Tracking

Table 2: Controller Parameters

Controller Properties	Values
P	34.4
I	21.6
D	3.0
N	3.7

Table 3: Controller Performance and Robustness

Performance Properties	Values
Rise Time	0.453 seconds
Settling Time	4.18 seconds
Overshoot	11.7
Peak	1.12
Gain Margin	6.21dB @ 44.6 rad/s
Phase Margin	87.3 deg @ 3.68 rad/s
Closed-loop Stability	Stable

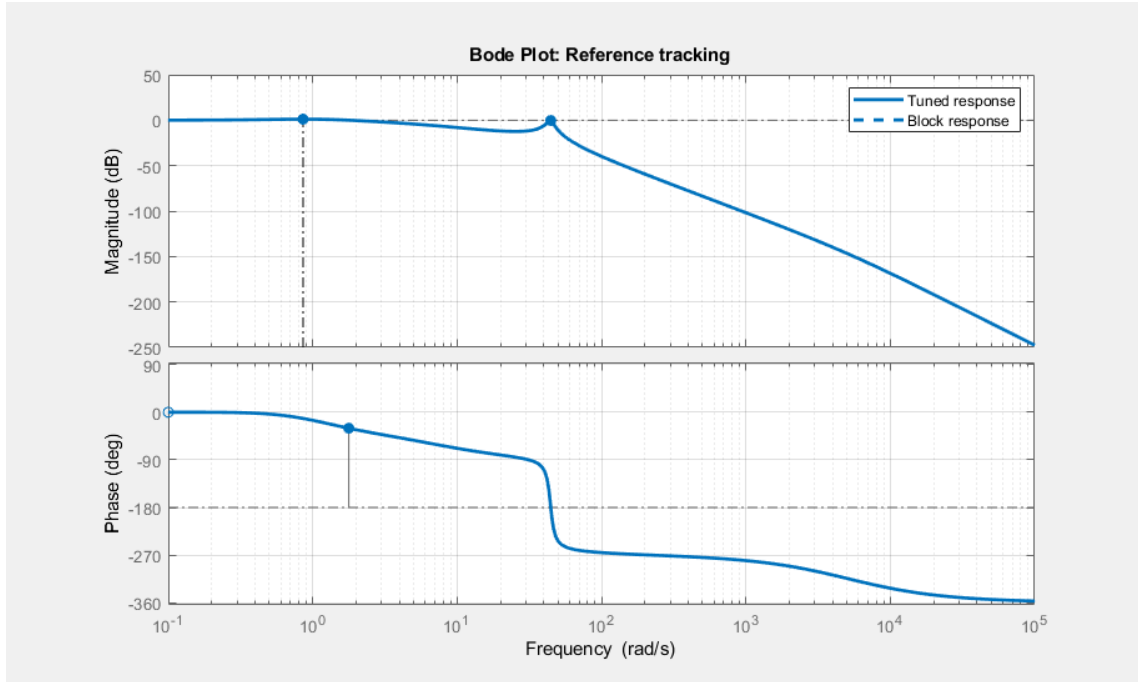


Figure 23: Controlled System's Bode Plot

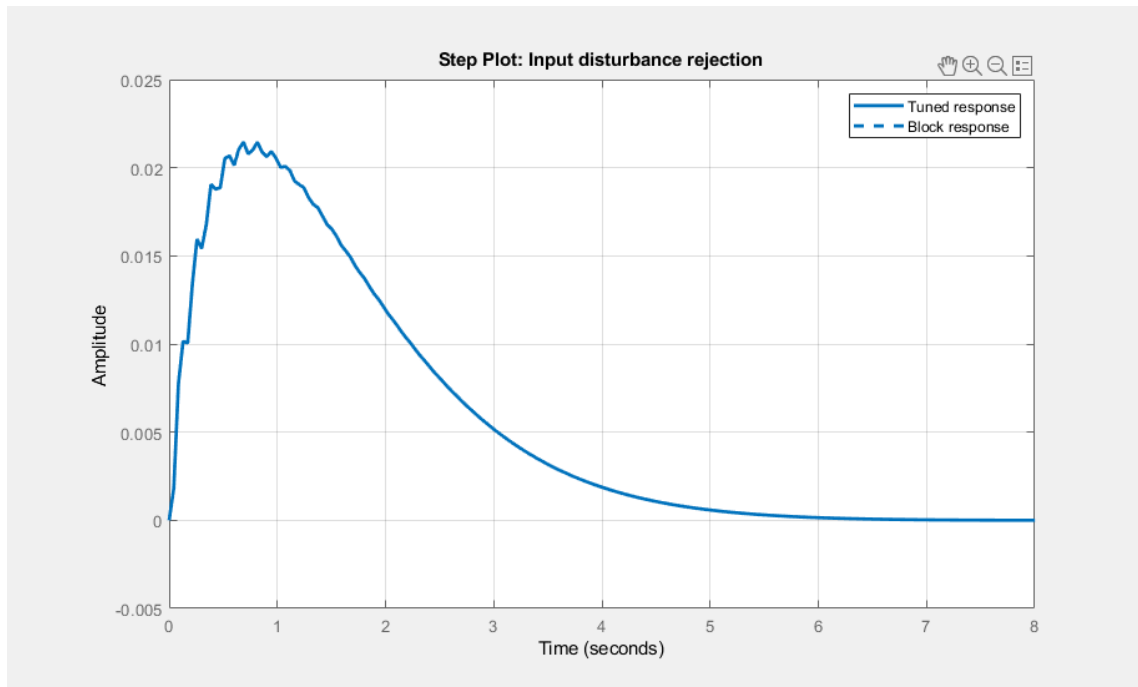


Figure 24: Input Disturbance Rejection

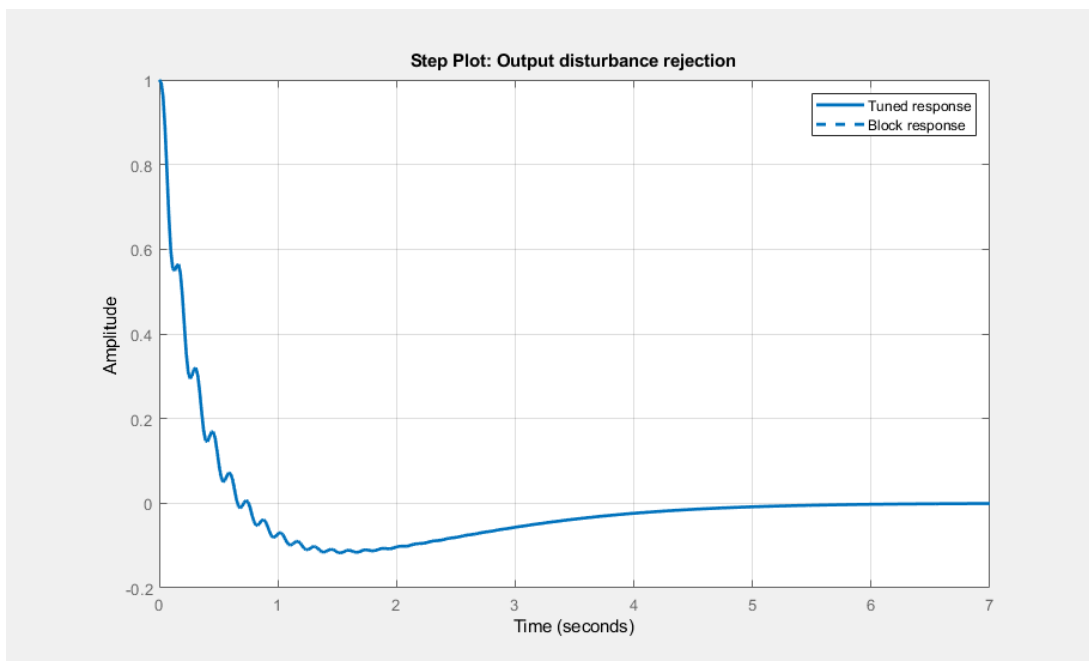


Figure 25: Output Disturbance Rejection

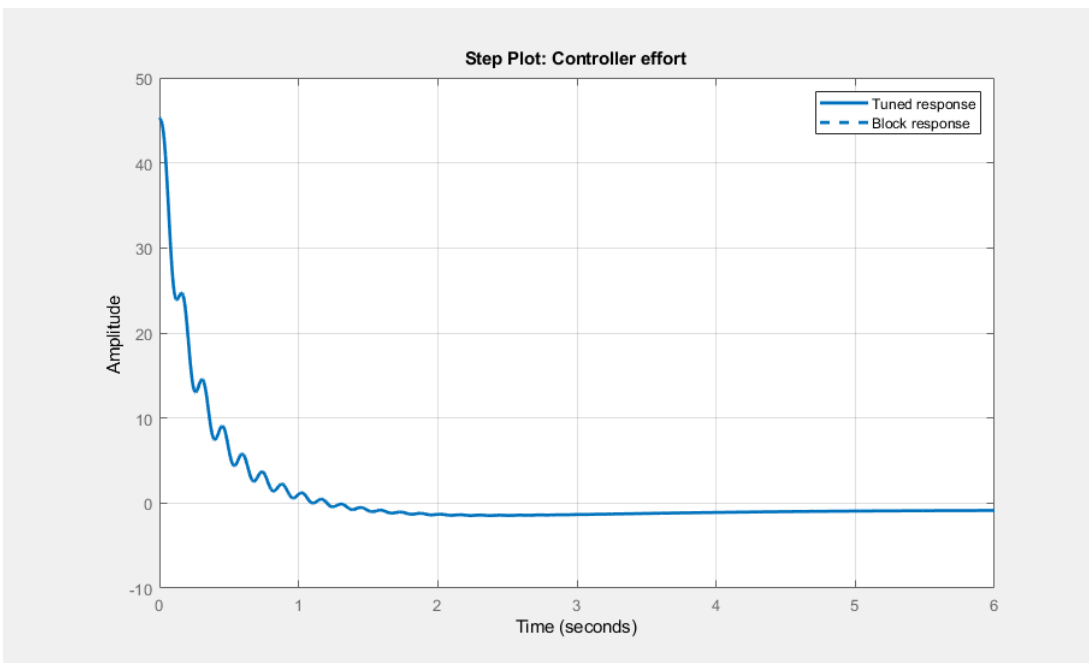


Figure 26: Controller Effort

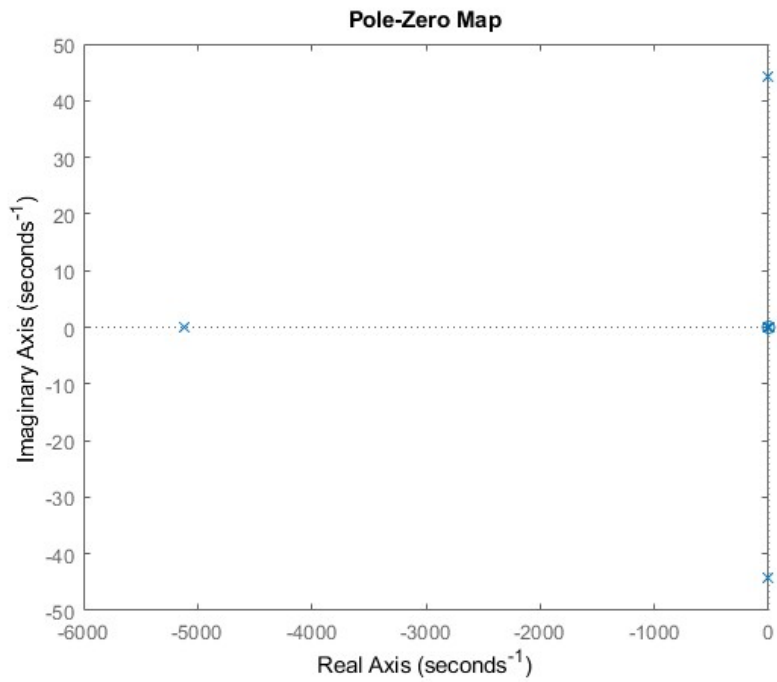


Figure 27: Controlled System's Pole Zero Plot

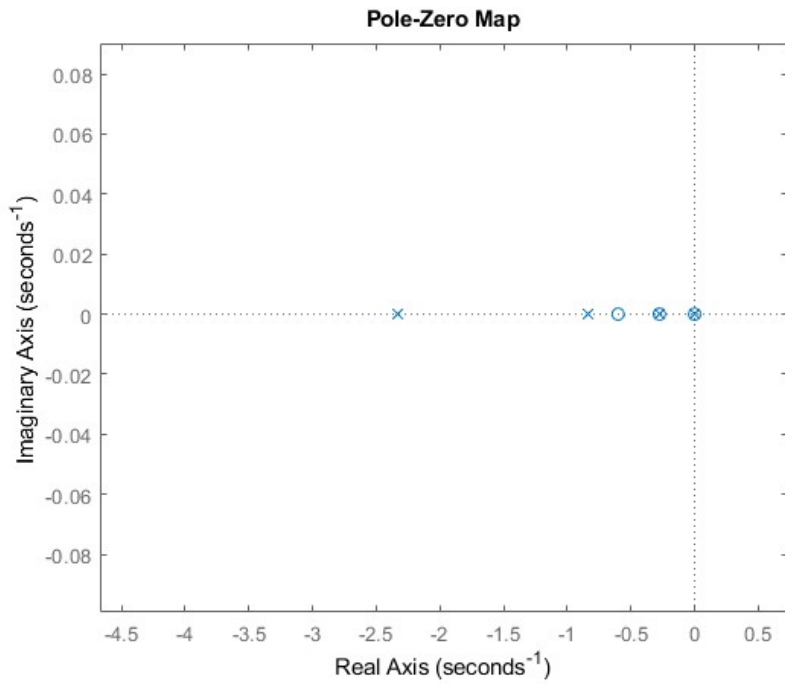


Figure 28: Controlled System's Pole Zero Plot (Zoomed)

3.4.3 Actuation Procedure

The gains that have been calculated above will only give us a starting point when we practically implement the controller specifications. These will be subjected to further changes when the Controller, IMU, and Servo Motor are connected together on the physical gyroscope system. The interface chosen to set and change the gains on the PID Microcontroller is LabView which allows for FPGA programming and can report back output and graphs with relative ease and high speeds [12].

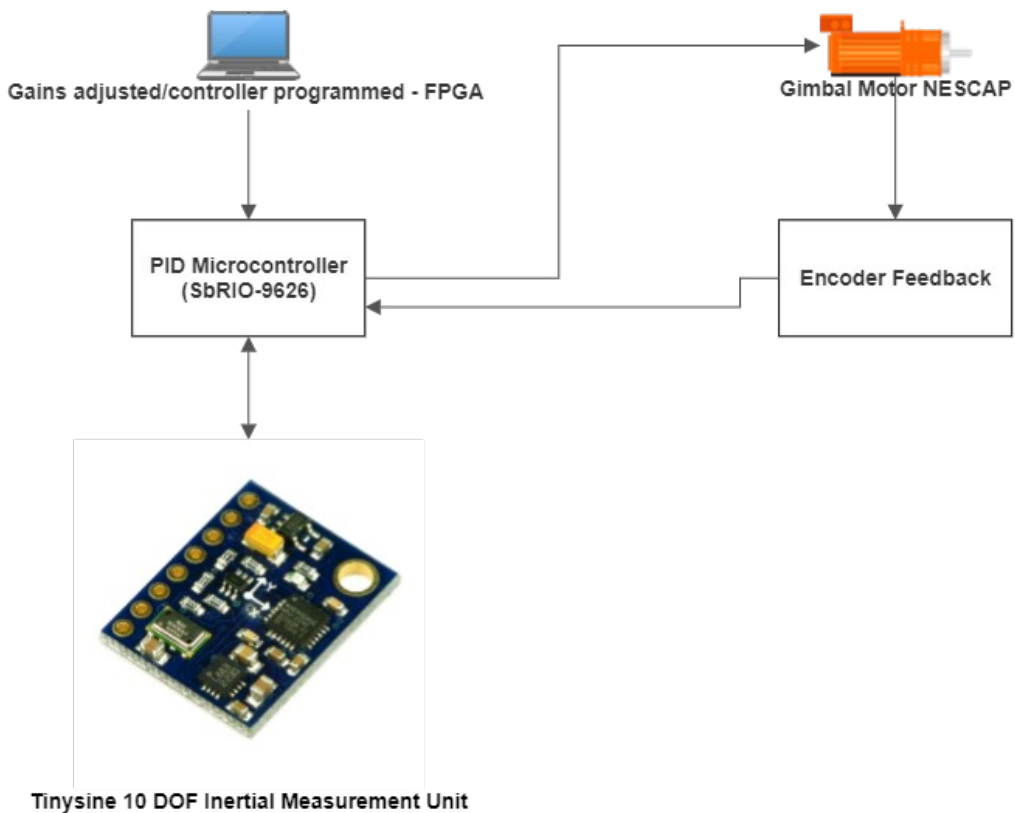


Figure 29: Physical Actuation Procedure

3.5 Mechanism Design Process

The aim of the design of this project is to enable motorcycle users to gain stability during driving. After initiating and executing the conceptual design, underlying equations, control systems and actuation, comes the 3-Dimensional design of the system.

3.5.1 Initial Designs

After thorough perusing of the literature review, various workable models for the motorcycle balancing attachment were brainstormed. The first design was inspired by the electric motorcycle variant and incorporated two vertical gyroscopes moving in opposite directions. The placement of this model was supposed to be beneath the motorcycle itself. This attachment had good torque capacity for the balancing purpose, however, it was a complex design and difficult to incorporate into the Honda motorbikes that are prevalent in Pakistan due to lack of adequate space underneath the main bike frame.



Figure 30: Initial Design Two Vertical Gyroscopes beneath Motorbike Frame

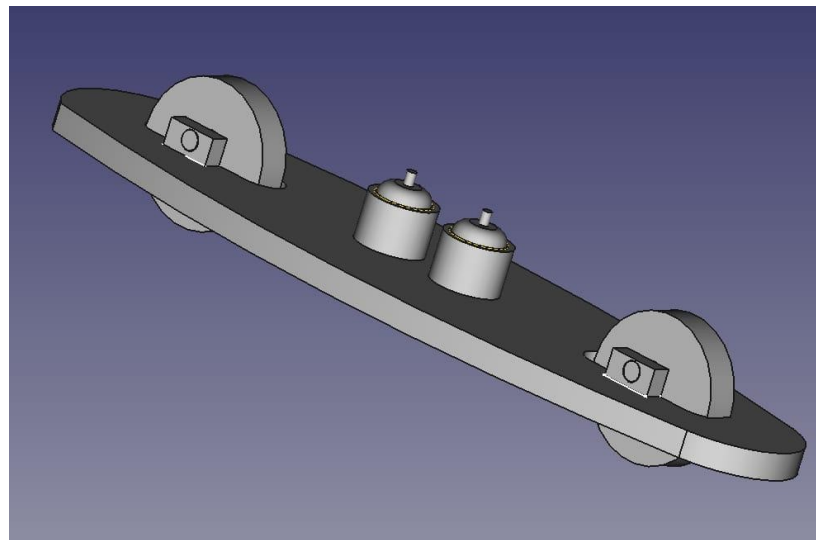


Figure 31: 3D Simplified Model of Initial Design

The second design consisted of a single vertical gyroscope that would provide torque for balancing while being attached to the front of the motorcycle. This version was

simple and less expensive than others, however, it had a major setback. This variant was not able to provide the torque capacity for balancing. It was only adequate for small children bikes and lightweight bicycles.



Figure 32: Initial Design with Single Vertical Gyroscope

The next design that was brainstormed was inspired by an experimental test bench. It consisted of a single gyroscope oriented along horizontal axis and it was placed at the back of the vehicle. Like the previous design, it was also simple and easy to fabricate, however, it offered minimal control when the team was developing its controls system. This alone rendered it un-useable as a potential design.



Figure 33: Initial Design with Single Horizontal Gyroscope

3.6 Final Design

The final model aimed to cover the shortcomings of all previous designs while being a workable mechanism. The 3D model was designed on Solidworks Pro. The model consisted of four major components. The hub motor was attached to thick metallic ring to constitute a self-moving gyroscope. This module was supported by a bracket that allows it to rotate and tilt freely while current is applied through the hub motor.

The bracket is supported on the main frame that is fixed to the body of the motorcycle. The rotation of the gyroscope is along the vertical axis of the bracket, meanwhile, the tilting occurs along the shared axis of the frame and bracket point of attachment. This test bench will be placed on the rear end of the passenger seat.



Figure 34: Isometric View of Model

3.6.1 Model Views

After finalizing the 3D model, a Solidworks Render was performed to get a final perspective of how the test bench would look in real life. Various views of the model are provided below to give a better understanding of each part and component.

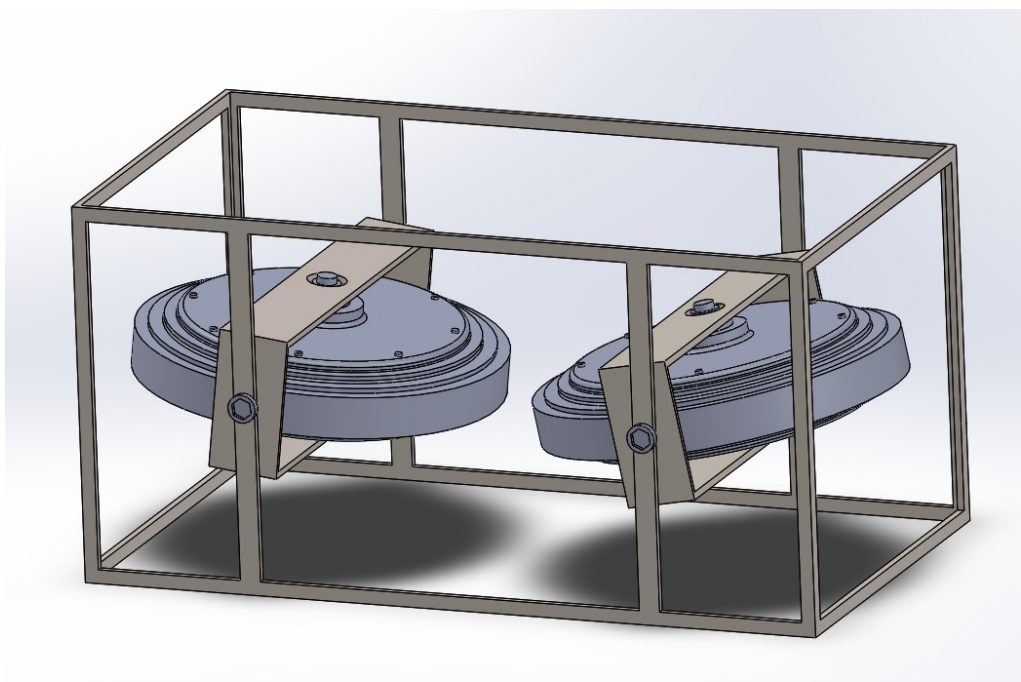


Figure 35: Modelling Design SolidWorks

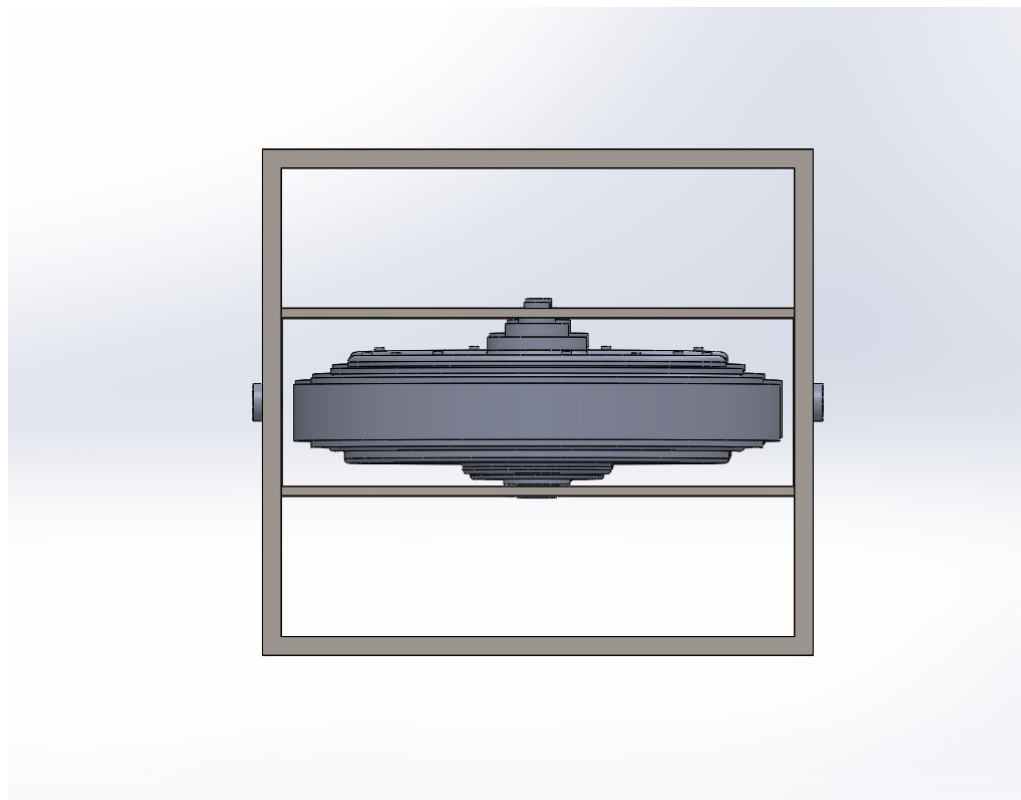


Figure 36: Assembly Side View

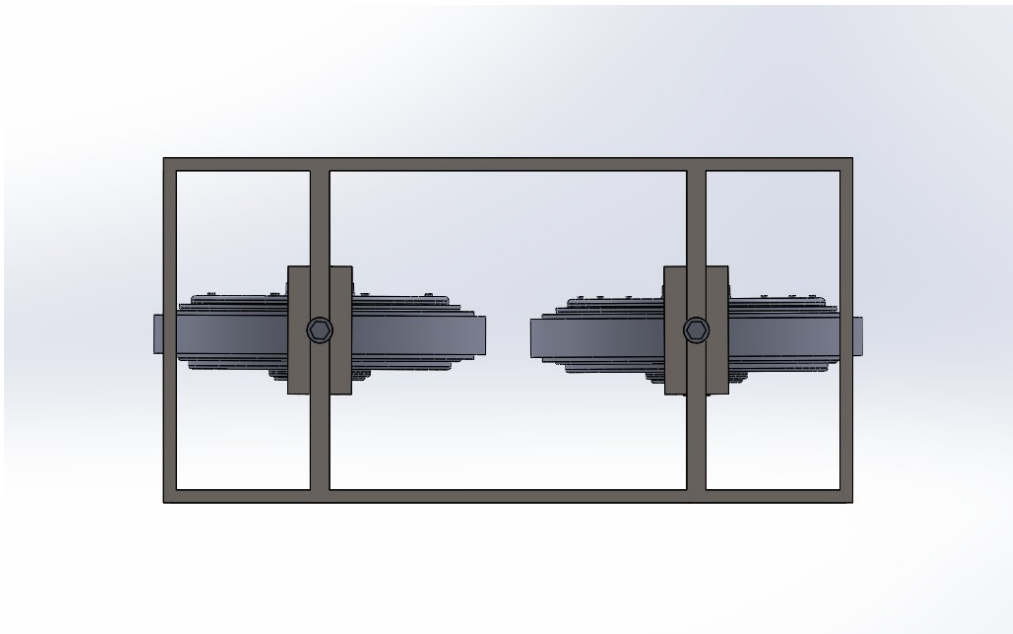


Figure 37: Assembly Front View

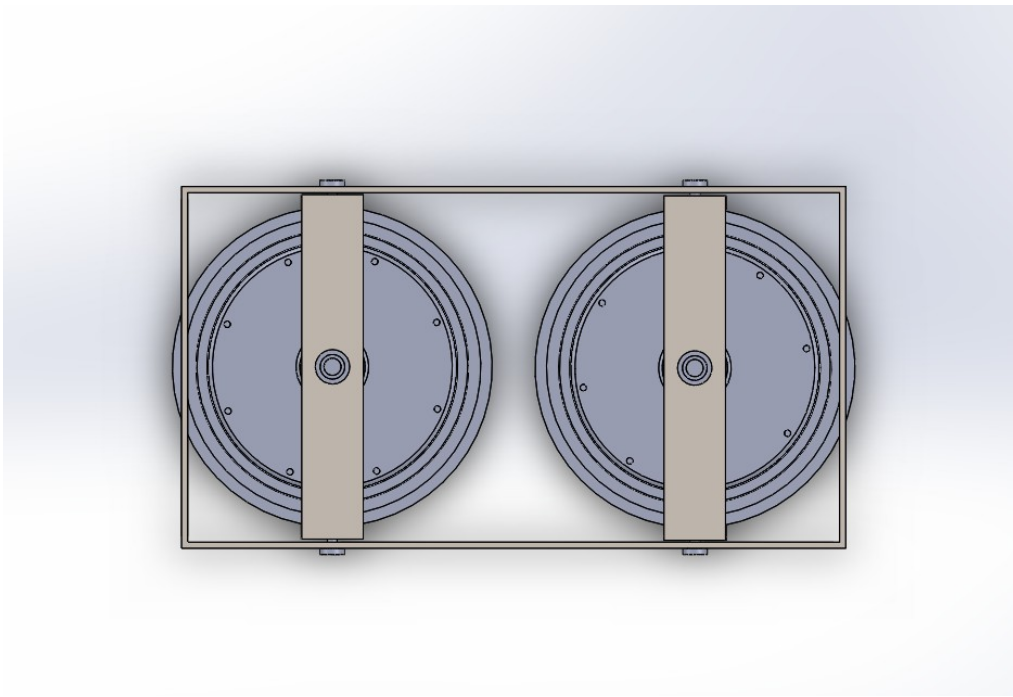


Figure 38: Assembly Top View

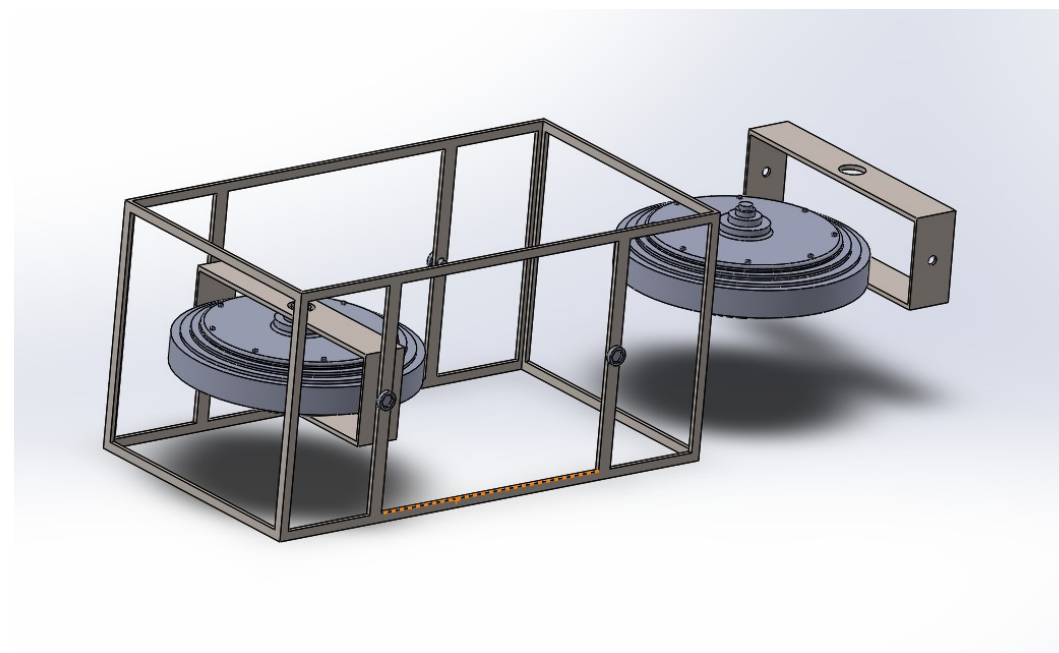


Figure 39: Assembly Exploded View



Figure 40: Side View Hub Motor



Figure 41: Hub Motor 3D View



Figure 42: Hub Motor Exploded View



Figure 43: 3D Model View



Figure 44: Model Placement on Vehicle

Special focus was placed on the Hub Motor part of the design and a quick exploded view was also provided to ensure that it is compatible with existing hub motor models that are available.

3.6.2 Part Dimensions

Moreover, a drawing of the model is also attached to provide information about the dimensions of each component as shown below. Detailed drawings are attached in APPENDIX VII: DETAILED PART DRAWINGS.

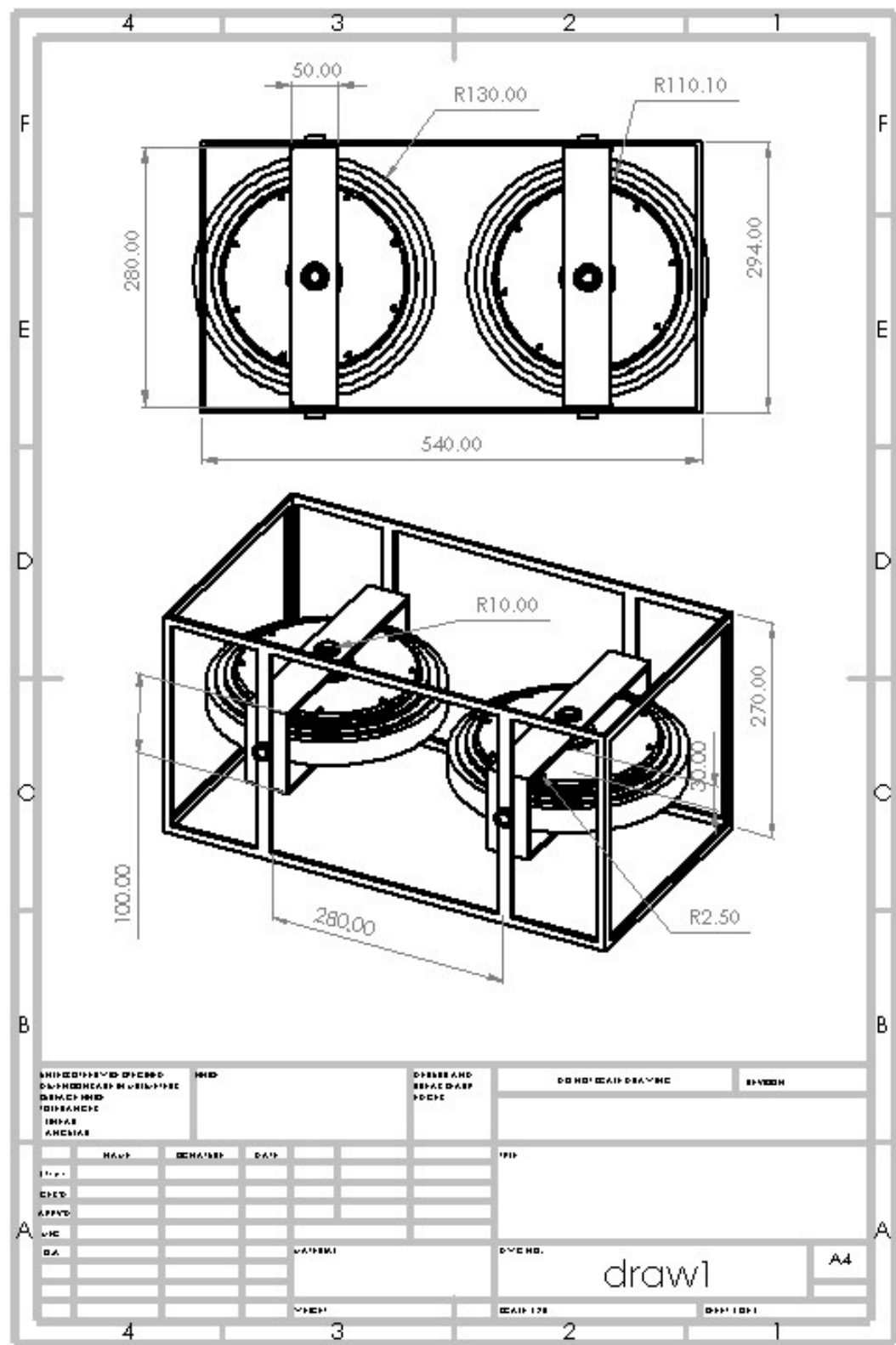


Figure 45: Drawing Specifications

3.6.3 Bolts Specification

The designed model utilizes 4x M10 bolts to connect the test bench to the frame of the motorcycle in a sturdy manner. The specifications of the bolts are given in the following table:

Table 4: Bolt Specifications

Dimensions		Areas		Tensile Resistance [kN]	Shear Resistance Per Shear Plane [kN]
Nominal Diameter [mm]	Nut Width Across Flats [mm]	Gross Area [mm ²]	Stress Area (Threaded Part) [mm ²]		
10	16	78.5	58	33.4	22.3

These specifications go in line with the proposed design. However, they can be modified depending on the model of the motorcycle which is being experimented on.

3.6.4 Nuts Specifications

M10 nuts were used to hold the M10 bolts in place on the motorcycle. Specifications are given in the table below:

Table 5: Nuts Specifications

Pitch [mm]	Proof Load [MPa]
1.5	580

3.6.5 Bearings Specifications

The formulated design uses 8 bearings to ensure smooth rotation of the gyroscopes and the tilting of the bracket due to the motors.

Bearing dimensions are attached in APPENDIX VI: BEARING DIMENSIONS

3.6.6 Material Selection

An important task before moving on to the analysis and simulation is to decide the

material of the design. In this section, the material used to fabricate the model is discussed. Some of the constraints faced in the material selection process were:

- a) The material should be such that the model does not undergo failure/crack during operation.
- b) The material should be such that the cost of the model is within reasonable range.
- c) Ease of commercial availability
- d) Ease of machining and fabricating

Considering these constraints, out of several available materials, Stainless Steel AISI 4340 was shortlisted for selection. Driving a qualitative and quantitative analysis, this material was most suited for the needs of the model. Specifications of this material that were used in calculations are mentioned as follow:

Table 6: Specifications of Stainless Steel AISI 4340

Property	Value	Units
Elastic Modulus	2.05×10^{11}	N/m ²
Poisson's Ratio	0.32	N/A
Shear Modulus	8×10^{10}	N/m ²
Mass Density	7850	kg/m ³
Tensile Strength	1.11×10^9	N/m ²
Compressive Strength		N/m ²
Yield Strength	7.1×10^8	N/m ²
Thermal Expansion Coefficient	1.23×10^{-5}	/K

3.7 Prototyping Cost Details

The detailed bill of materials is attached in APPENDIX V: BILL OF MATERIALS. A preliminary analysis on those front shows that the max cost of the design comes out to be Rs. 305,000 approximately. This includes all purchases, machining, and assembly costs.

Compared to the prices of the counterpart designs already present in the market, the model is well within financial limits and significantly cheaper. Moreover, the cost is expected to be lower than this if mass production is considered.

3.8 Summary

In this chapter, the following main points were discussed:

- Dynamic Modelling (deriving equations of motion)
- Obtaining solutions of the derived system
- Verifying the instability of the derived system
- Designing a control system to stabilize the derived set of equations.
- Brainstorming various models for our designs
- Finalizing the design
- Part details
- Drawings and specifications
- Estimated cost of test bench.

CHAPTER 4: RESULTS AND DISCUSSIONS

4.1 Introduction

A very significant part of the design is to validate the structural model using Finite Element Analysis methods. There are a multitude of software that are available today for various FEA simulations.

Analysis of the model was performed on COMSOL 5.6 using Multibody Dynamics Physics and Time Dependent Study initially. This model was considered as the final candidate to be taken for FEA as it was not only optimized to the project's requirements but also addressed all stability issues. Solidworks Simulations was also utilized as a platform for our analysis since our 3D model was designed on this software.

In this chapter, FEA will be documented and discussed in detail. First and foremost, mesh convergence analysis to determine the optimum mesh density for the proposed design will be discussed. It will be followed by simulation results of each part and its consequent discussion. The completion of this stage will be followed by the analysis of the model on COMSOL and Solidworks while prescribing appropriate boundary conditions.

During the analysis process, it was aimed to check the Von Mises stress in each part against the yield strength of the material. The Von Mises stress is used as a suitable criterion for comparison of results as it provides comprehensive distortion energy in a material by showing change in shape which is a much better and accurate representation of yield testing.

The assembly has primary supporting joints. Two gyroscopes are nestled in the support bracket with the help of bearings which connect the hub motor shaft with the bracket. Similarly, the bracket is maintained in place in the main frame with the help of 2 bearings each. The bracket is connected to the servo motor which allows the tilting motion of the bracket. Simple force analysis reveals the magnitude of the forces/torques at these joints and allows for the parts to be analyzed separately.

4.2 Part Analysis

For each part, as discussed before, mesh convergence analysis on Solidworks was manually performed to check mesh density until two consecutive results had minimal

difference. This allowed saving on the computational power required by not choosing extremely fine mesh density.

4.2.1 Main Frame

Beginning sequentially, first the main frame is analyzed which is housing the whole setup withing. The 3D model meshing is displayed both with initial coarse meshing and final fine meshing setup.

The boundary conditions are also specified to give accurate results. The material assigned is AISI 4340 Steel. The lower face of the frame was constrained as fixed geometry as it would be stationary with respect to the motorcycle. Moreover, the forces and torques were calculated at the joints shown in the figure. Torques were applied at the hole surface keeping in mind the bearing load and diameter of the hole.

The analysis was performed in Solidworks Pro Simulation and the aim was to obtain Von mises stress, strain, and model displacement.

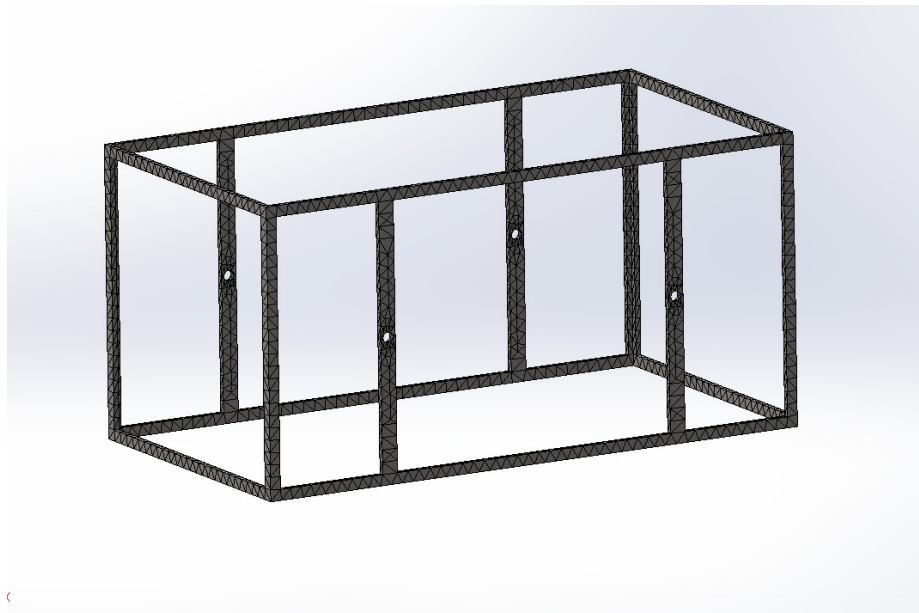


Figure 46: Main Frame Coarse Meshing

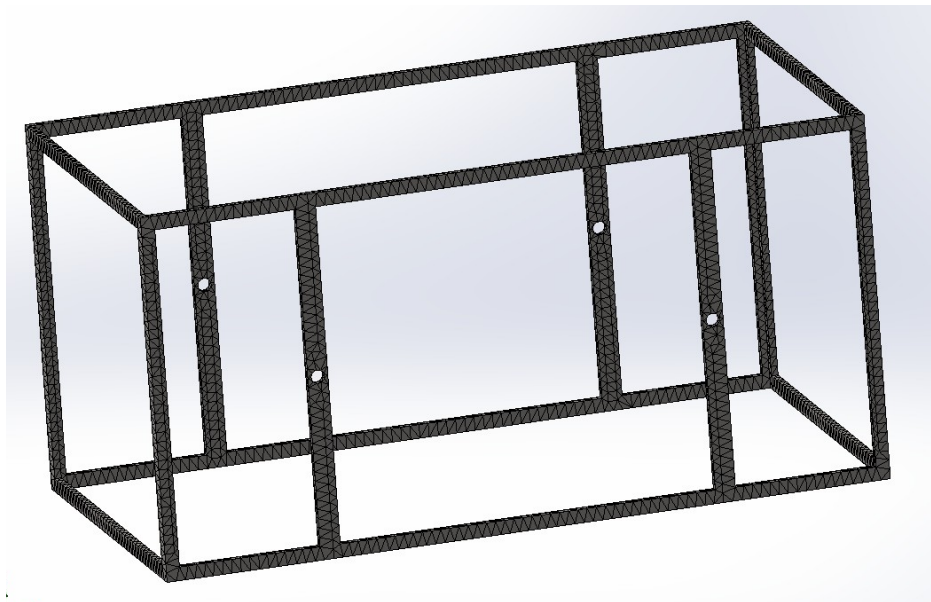


Figure 47: Main Frame Fine Meshing

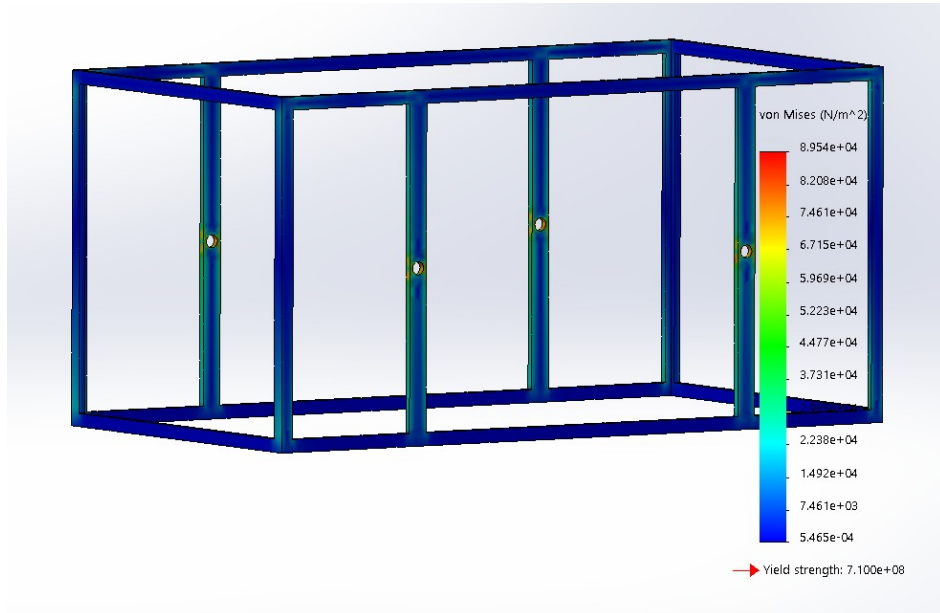


Figure 48: Frame Von Mises Stress Analysis

The results of the study show that all the stresses that were imminent in the model were well below the yield strength of the material. They also conformed to the factor of safety of 1.1. The boundary conditions were based on the extreme loading conditions and the resulting simulation denotes that even in worst case scenario, the model would not be undergoing failure.

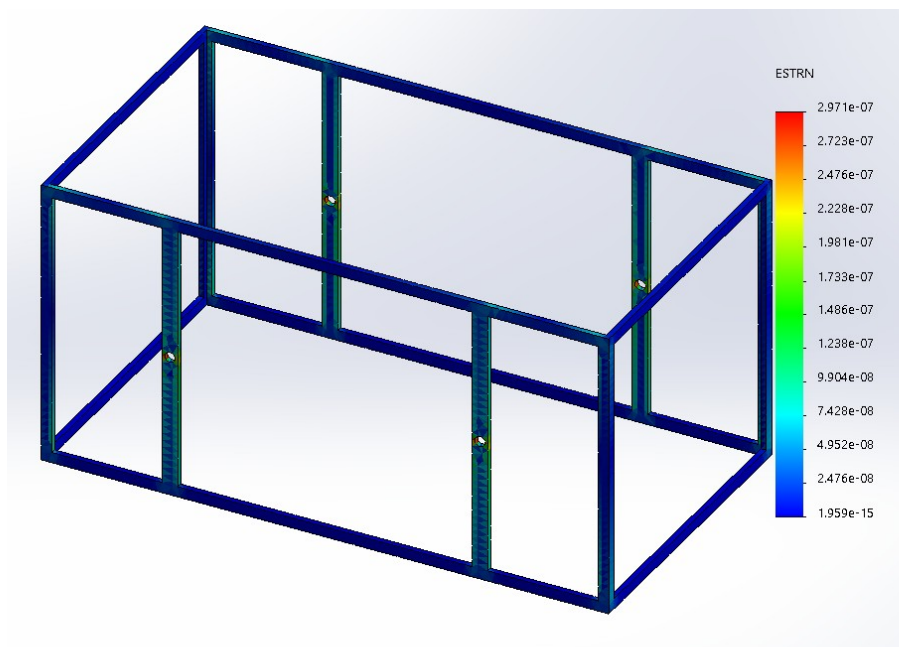


Figure 49: Main Frame Strain Analysis

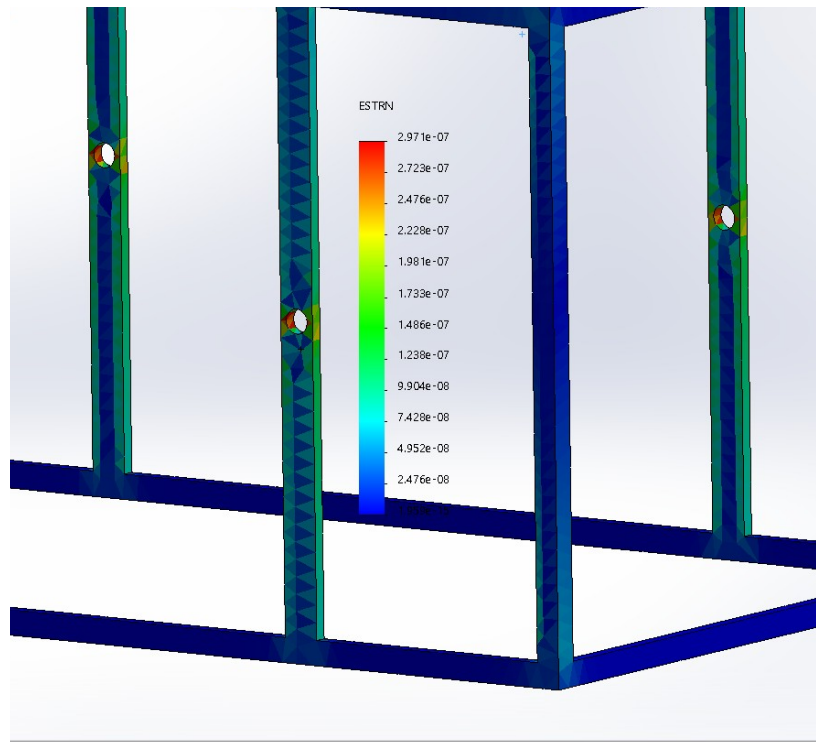


Figure 50: Main Frame Strain Analysis Close-up

The strain analysis results also show that the model is very stable under harsh loading conditions and the strain is very negligible. The results also agree with the predictions taken before running the simulations.

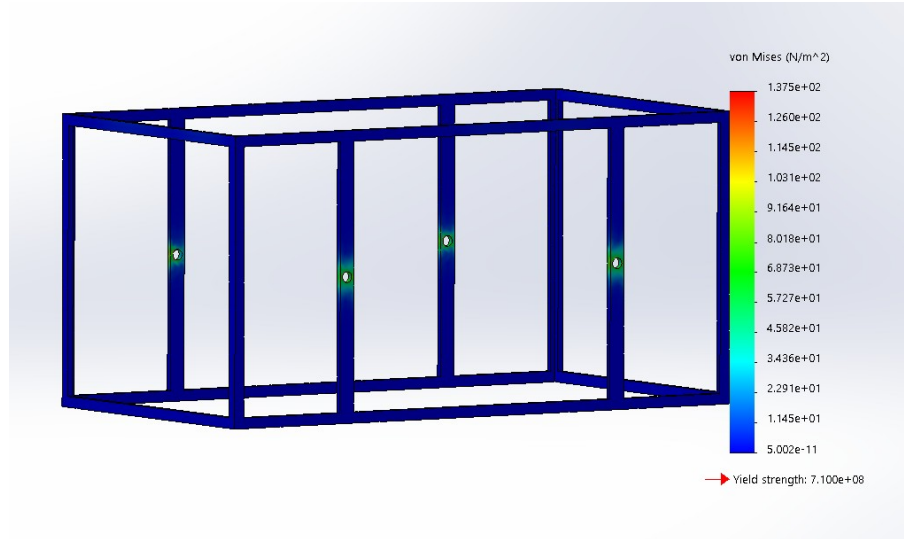


Figure 51: Main Frame Vibrational Stress Analysis

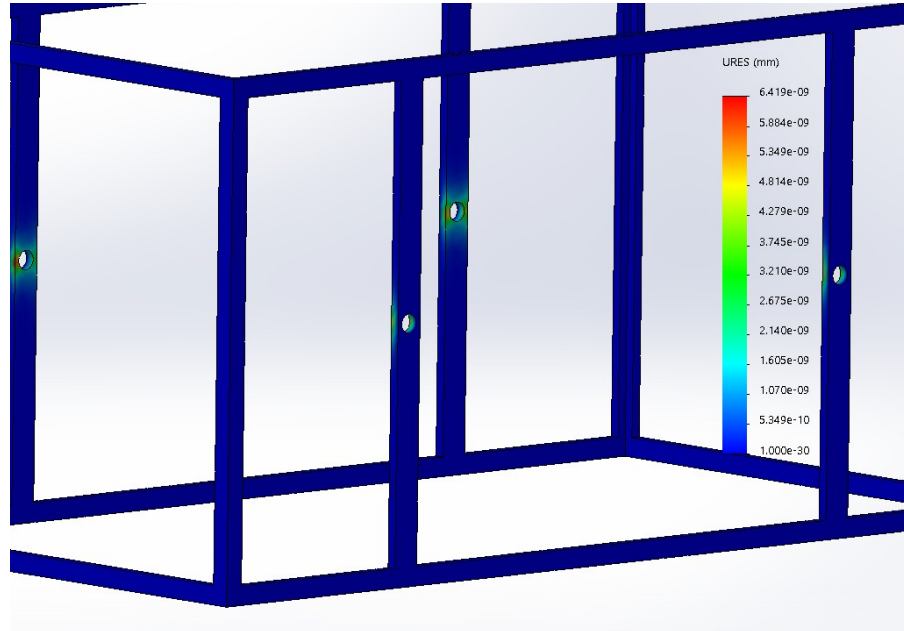


Figure 52: Main Frame Vibrational Strain Analysis

Since this test bench would be utilized on a motorcycle, another important study was Vibrational stress analysis. As a motorcycle moves on an uneven road, it experiences true random vibrations, and it is important to translate the effect of such vibrations on the body of the model to ensure there is no chance of resonance. For this purpose, a random jerk due to velocity change was applied and results were noted. As predicted, the model showed stress at joints only and the stress & strain were well within the prescribed limit. Overall, the part study for the main frame was successful.

4.4.2 Support Bracket

The next part that was analyzed was the support bracket that was responsible for holding the gyroscope attachment inside the main frame. The design used 2 such brackets for each gyroscope. The point of load application is greater on this part. The sides are supported by the main frame with bearings and motor. The top and bottom faces support the hub motor shaft with the aid of bearings.

The material applied was the same as the main frame, AISI 4340 structural steel. The torques applied were calculated and applied as the boundary conditions. The inner face was constrained to give better results and hold the geometry in place. Mesh convergence was also checked to ensure the appropriate mesh density for simulation results.

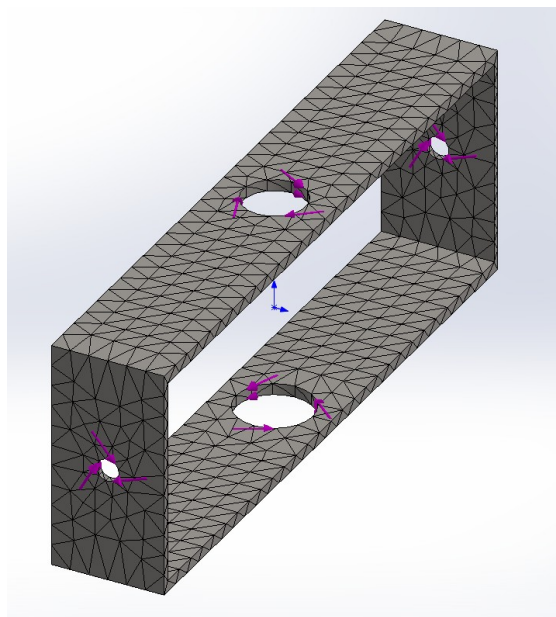


Figure 53: Support Bracket Coarse Mesh

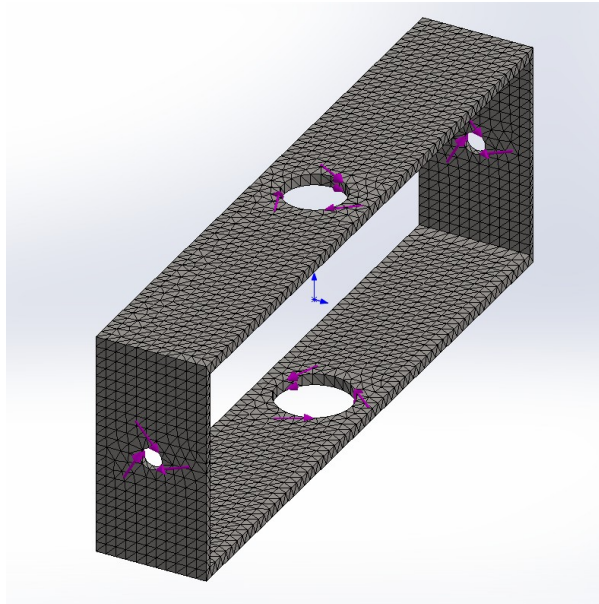


Figure 54: Support Bracket Fine Mesh

The analysis was performed on Solidworks Pro Simulation environment. As predicted, the results showed stresses only at certain locations on the body of the part. However, these stresses were very low compared to the yield strength of the material leading to the conclusion that the part would not deform or fail even under worst-case scenarios.

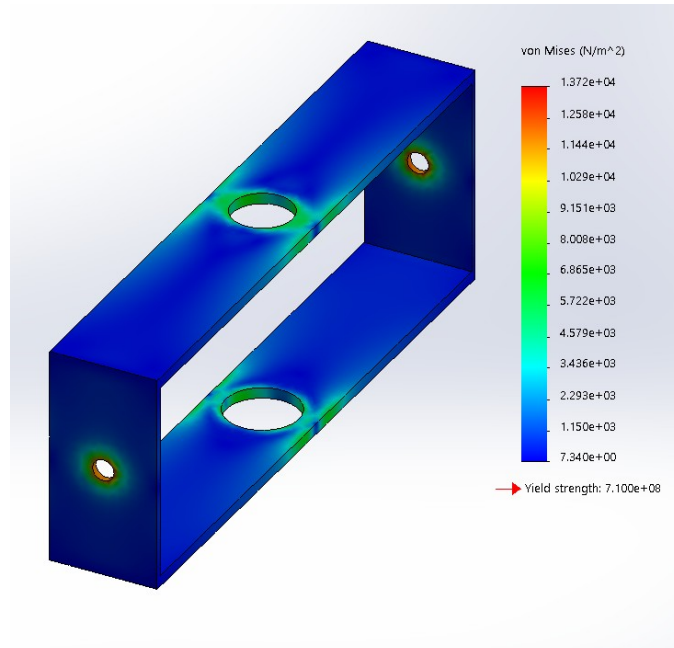


Figure 55: Support Bracket Stress Analysis

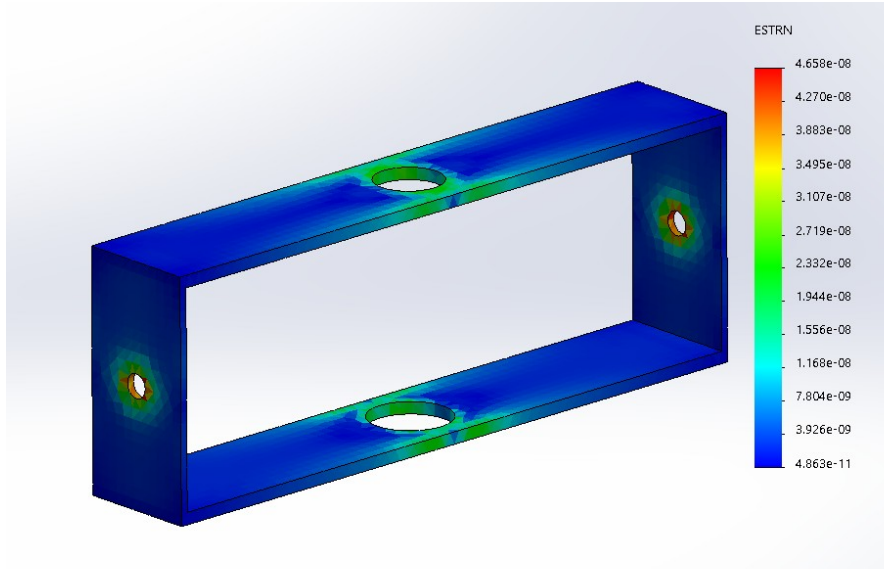


Figure 56: Support Bracket Strain Analysis

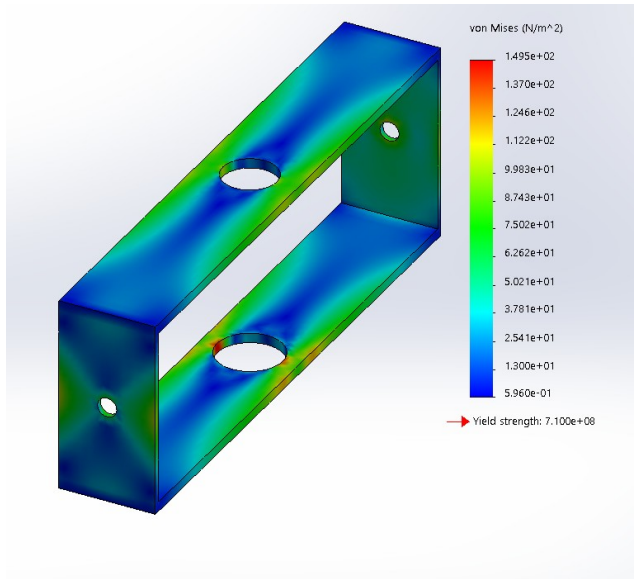


Figure 57: Support Bracket Vibrational Stress

A vibrational stress analysis was also performed for the support bracket under the same boundary conditions as the main frame to replicate the results of sudden jerks on an uneven road as the motorcycle is driving. As predicted the results showed that due to a sudden jerk, there would be a certain loading on the joints of the support bracket that would cause stress to spread evenly out throughout this bracket. These stresses are different than the ones in the previous analysis as not only the weight of the hub motor-gyroscope and the support bracket is involved in this but also the jerk due to the vibration causes extra stress of the hub motor gyroscope attachment to be exerted on the joints.

However, these results and stresses are way below the limit of the material itself which concludes that there would be no failure in the material. Overall, the study is considered successful for this specific part.

4.4.3 Gyroscope Attachment

The last stage of the component analysis was for the gyroscope hub motor attachment. In this analysis the hub motor and the gyroscope were taken as single part to simplify Von mises analysis as well as vibrational stress analysis. As discussed before, this attachment was supported between the two faces off the support bracket with the help of bearings and similarly loads were calculated that were to be applied on the shaft of the hub motor.

First, an appropriate mesh density was established on this attachment and then suitable torque loadings were applied on the shaft. The material off this gyroscope was the same as the previous parts. The shaft of the hub motor was constrained as fixed geometry to yield accurate results. For vibrational stresses similar boundary conditions were applied to check the effects of sudden vibrations of the road on the gyroscope attachment. The base excitation was provided in the form of a velocity change. Since this is rotating at very high speeds, centrifugal force is also applied to check the effects of high rotational speeds on the body of the gyroscope

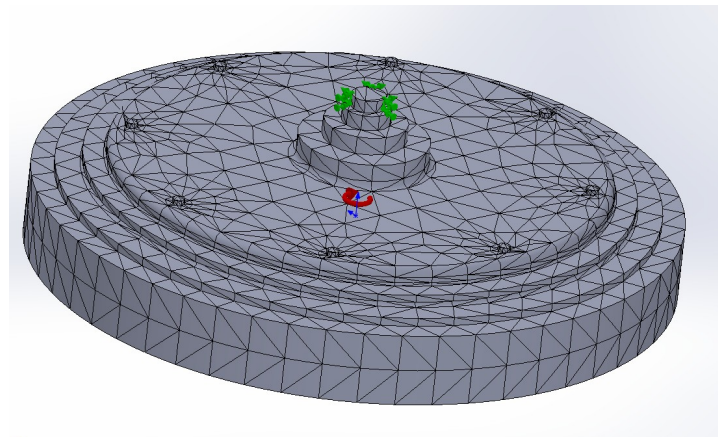


Figure 58: Gyroscope Coarse Mesh

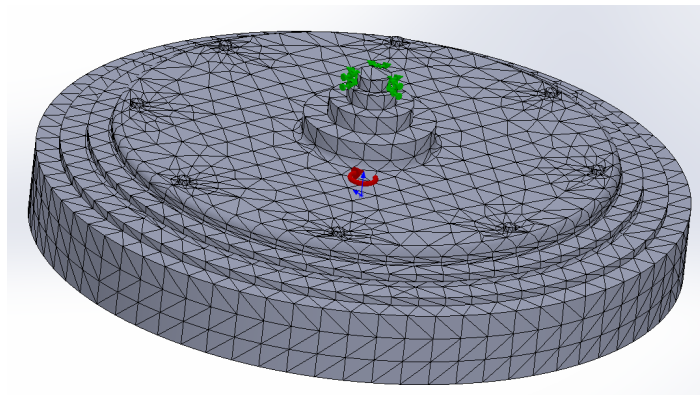


Figure 59: Gyroscope Fine Mesh

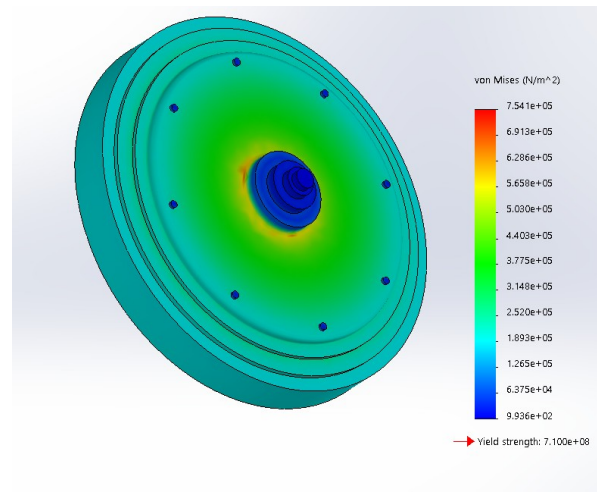


Figure 60: Gyroscope Stress Simulation at High Speeds

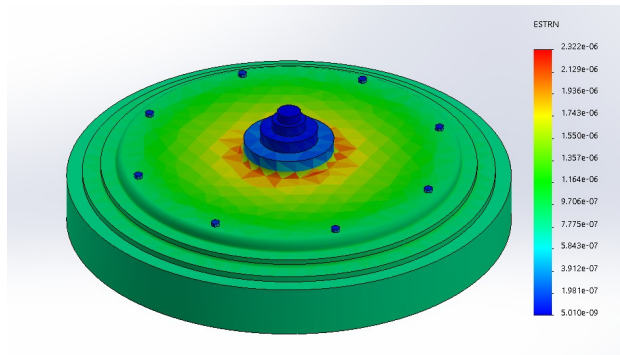


Figure 61: Gyroscope Strain Analysis at High Speeds

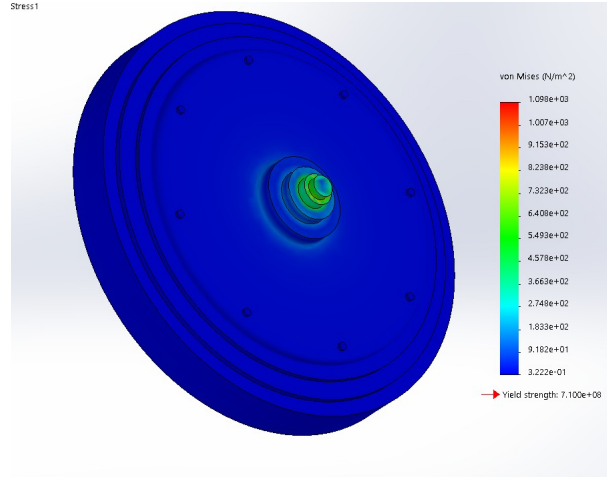


Figure 62: Gyroscope Vibrational Stress Analysis

The analysis was carried out on simulations SolidWorks. As predicted, the results show that all the stresses in the body of the gyroscope attachment are way below the yield limit of the material itself. This shows that there would be zero failure occurring even at worst case scenario. At high rotation speeds, the stress is also distributed evenly throughout the body of the gyroscope attachment. This aligns with our predicted results. Coming on to the results of the vibrational stress analysis, it is noted that due to sudden vibrations, the loading would be the most at the shaft of the hub motor. However, that stress value is very low compared to the yield strength of the shaft material. It can be concluded that the study for the gyroscope attachment is successful.

4.3 Assembly Analysis

Once the analysis and design were completed for individual parts and the element size for mesh convergence obtained, the next step was to conduct a multibody analysis as a whole assembly. This process would provide more accurate results as compared to the analysis of the individual parts because they were analyzed under approximate boundary and loading conditions.

When mesh density was checked at coarse mesh density, the model failed to generate a mesh due to small parts of the gyroscope attachment. Therefore, there was a need to reduce the mesh density that a finer mesh would be generated for accurate results. It is important to note that the support brackets had tilting motion with respect to the main frame and the gyroscopes were also provided free rotational capabilities with respect to

the support bracket. These boundary conditions were applied to ensure a workable model that could be simulated in the COMSOL environment.

The analysis was performed in the SolidWorks and COMSOL Multibody Dynamics environment to see the Von Mises stresses, velocities, and displacements.

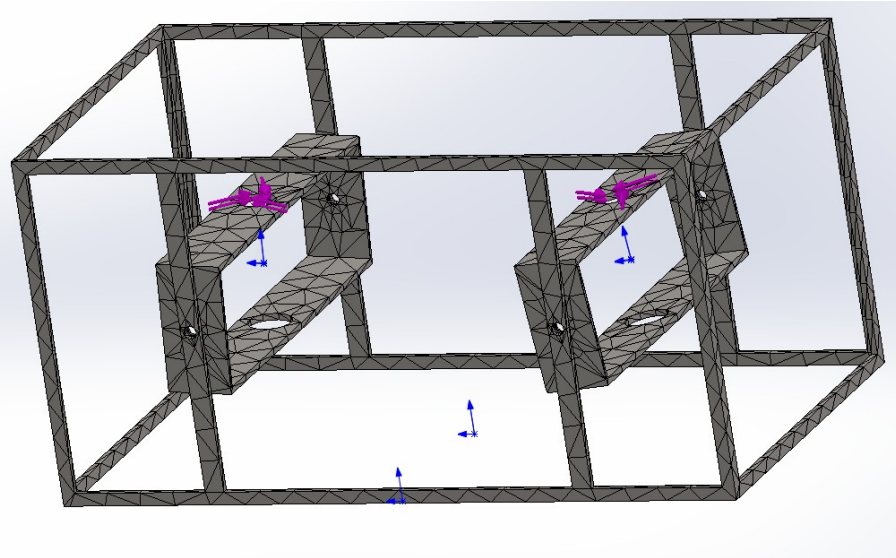


Figure 63: Coarse Mesh Assembly

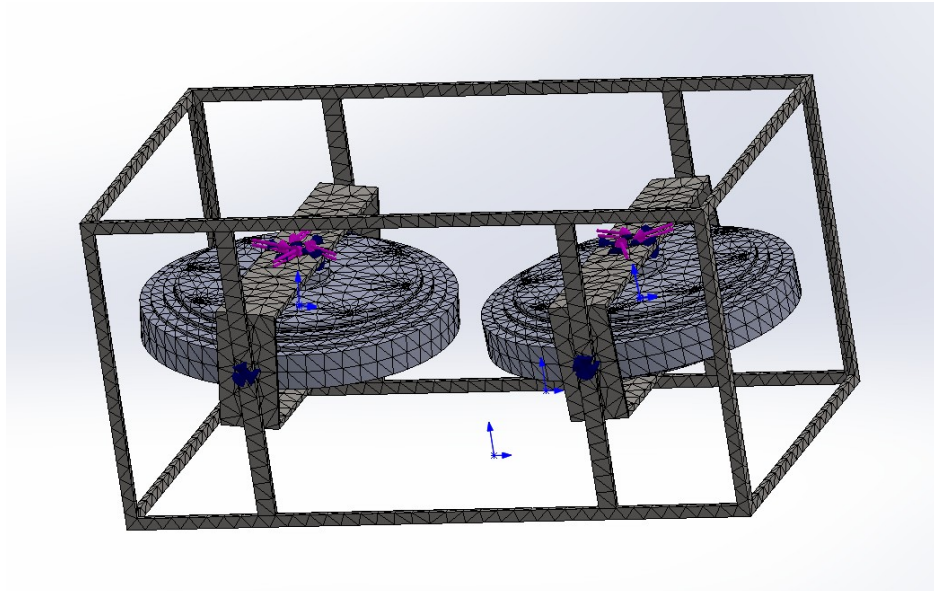


Figure 64: Fine Mesh Assembly

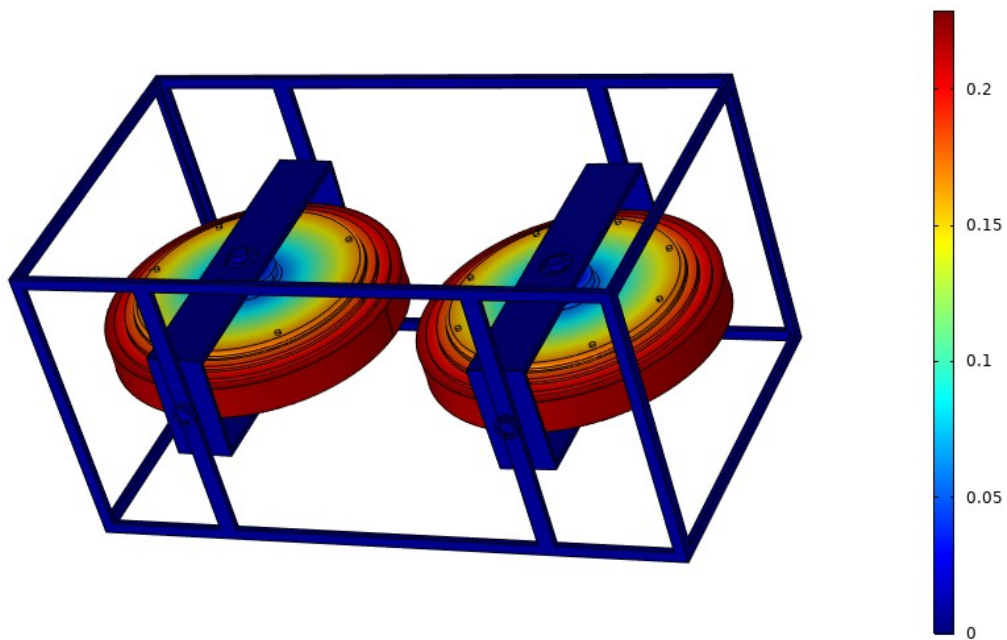


Figure 65: Displacement Magnitude (m)

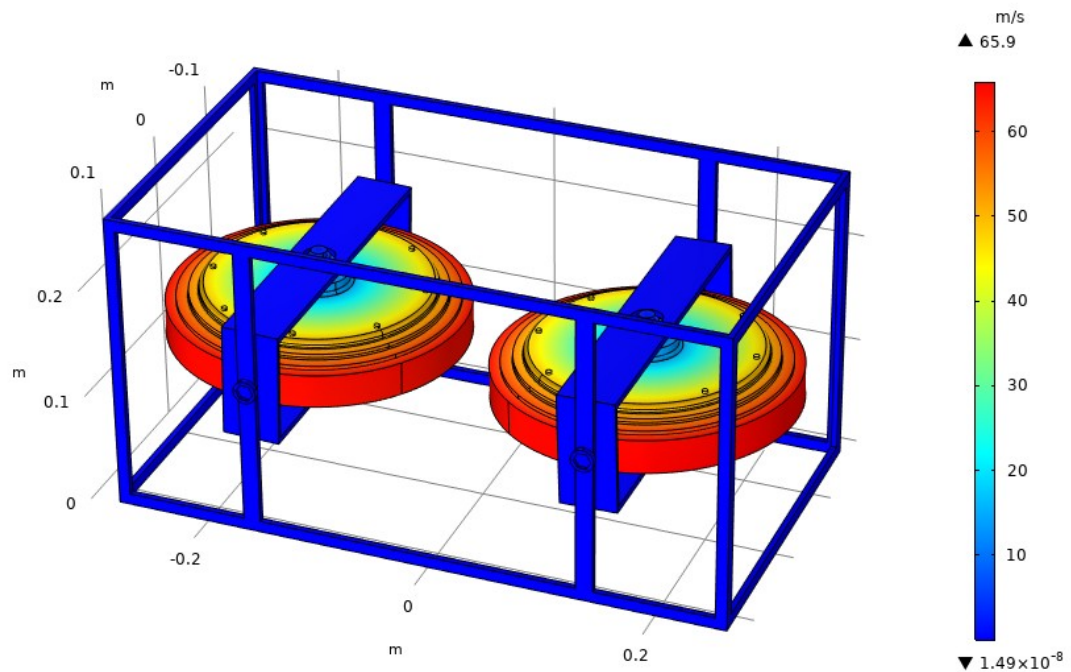


Figure 66: Velocity Magnitude

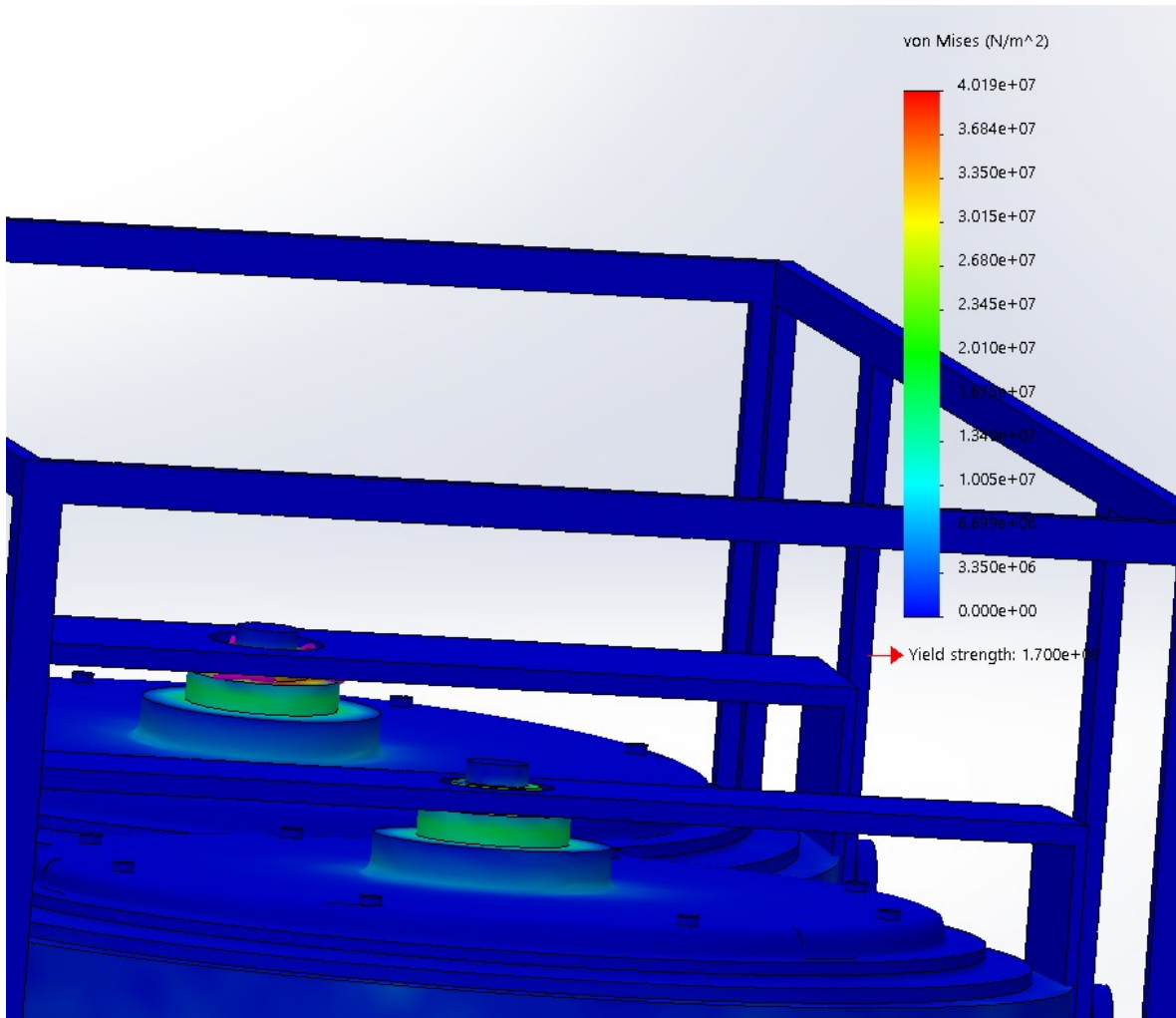


Figure 67: Von Mises Stress

The simulation results agreed with control system design and mathematical calculations, with all parameters being within acceptable range while the gyroscopes are in operation.

Constraints applied were limiting parameters as maximum velocity and torque was applied to observe if there was any failure at maximum capacity of operation. The results show that the model shows no material failure, and the model remains intact during the entirety of the working.

This brings the conclusion that the design is feasible for high speeds and torques and will not fail under vibrational stresses.

CHAPTER 5: CONCLUSIONS AND RECOMMENDATIONS

To achieve the goals of this project, a very systematic approach was adopted to move towards results. To track the progress of the project, several milestones were placed and monitored. A thorough literature review was conducted, and all the relevant information was extracted that would provide a good foundation for the project domain. Models that were already in execution or in experimental phase were also investigated and an effort was made to find a way to apply them to the problem statement in hand. The objectives and constraints that were defined in the beginning of the project were the focal point of every design decision taken during the tenure of this project. Various actuation techniques, material choices and implementation methodologies were looked upon before finalizing a single approach. This was done mostly keeping in view of the conclusion and results of the equations derived for the model. Extensive analysis was performed as part of the research and analysis phase of the project. 3D models of the attachment were created using modern engineering software like SolidWorks. Each part of the design modelled was then analyzed under the specified loadings to ensure the body stresses and material deformation would not cause any problems for the attachment, the motorcycle and most of all the person operating it. The analysis was carried out in two software environments: COMSOL and SolidWorks. The effects of high torque, vibrations and rotational motion were analyzed across the whole design.

All main objectives and deliverables of the project were achieved. The project aided in the amalgamation of mathematical modelling, control systems, electrical circuitry, and mechanical actuation to create a unique product for the betterment of society.

The in-depth research and workings on this project have led the team to the following recommendations for the self-balancing two-wheel vehicle attachment using mechanical gyroscopes.

- The gyroscope design for achieving stability has been modelled correctly to operate on a Honda motorcycle which is extremely prevalent in the Pakistani landscape. This renders the model workable and easy to implement to aid people with lower limb disabilities.

- The implementation of the gyroscope model on the motorcycle is projected to improve the safety ratings of the locally produced Honda motorbikes.
- The stability of the model will improve the handling and usage of the motorcycle by the user.
- As a result of improved maneuverability, the number of accidents caused due to loss of balance of motorcycle on the road will be reduced drastically.
- It is recommended that Honda Atlas take up this opportunity to add this stability feature with their motorcycles and perform thorough testing of this attachment to give a more robust, stable, and safe driving experience to its users.

REFERENCES

- [1] A. Akhtar, M. Shoaib and A. Shami, "Motorcycle Accidents, A Real Burden & Challenge of Health," *Journal of Islamabad Medical & Dental College*, pp. 95-99, 2017.
- [2] H. Akhtar, "ROAD SAFETY SITUATION IN PAKISTAN," 2016.
- [3] K. Mishra, V. Siddharth, P. Bhardwaj, A. Elhence, D. Jalan, P. Raghav and S. Esam Mehmood, "The Prevalence Pattern of Locomotor Disability and its Impact on Mobility, Self-Care, and Interpersonal Skills in Rural Areas of Jodhpur District," *Nigerian Medical Journal*, pp. 156-160, 2019.
- [4] F. A. Rathore, S. B. Ayaz, S. N. Mansoor, A. R. Qureshi and M. Fahim, "Demographics of Lower Limb Amputations in the Pakistan Military: A Single Center, Three-Year Prospective Survey," *National Library of Medicine*, 2016.
- [5] M. Bayly, M. Regan and S. Hosking, "INTELLIGENT TRANSPORT SYSTEMS AND MOTORCYCLE SAFETY," Monash University Accident Research Centre, 2006.
- [6] A. Beznos, A. Lenskij, A. Formal, A. Grishin, D. Okhotsimskij, E. Gurfinkel, D. Jicharev, A. Savitsky and L. Tchesalin, "Control of Autonomous Motion of Two-wheel Bicycle with Gyroscopic Stabilization," *IEEE*, pp. 2670-2675, 1998.
- [7] S. Lee and W. Ham, "Self Stabilizing Strategy in Tracking Control of Unmanned Electric Bicycle with Mass Balance," *IEEE*, pp. 2200-2205, 2002.
- [8] Y. Tanaka and T. Murakami, "Self Sustaining Bicycle Robot with Steering Control," *IEEE*, pp. 193-197, 2004.
- [9] J. M. Gallaspy and J. Y. Hung, "Gyroscopic Stabilization of an Unmanned Bicycle," Auburn University, 1999.
- [10] M. Romano and B. N. Agrawal, "Attitude Dynamics/Control of Dual-Body Spacecraft with Variable-Speed Control Moment Gyros," *JOURNAL OF GUIDANCE, CONTROL, AND DYNAMICS*, vol. 27, no. 4, pp. 513-525, 2004.
- [11] X. Roser and M. Sghedoni, "Control Moment Gyroscopes (CMG's) and their Application in Future Scientific Missions," *Spacecraft Guidance, Navigation and Control Systems, Proceedings of the 3rd ESA International Conference*, pp. 523-

528, 1996.

- [12] P. Y. Lam, "Design and Development of a Self-Balancing Bicycle using Control Moment Gyro," *IEEE*, pp. 247-251, 2011.
- [13] N. Bedrossian, S. Bhatt, W. Kang and I. Ross, "Zero-propellant Maneuver Guidance: Rotating the International Space Station with Computational Dynamic Optimization," *IEEE Control Systems Magazine*, vol. 5, no. 29, pp. 55-73, 2009.
- [14] H. Goldstein, C. Poole and J. Safko, *Classical Mechanics*, Addison-Wesley, 2001.
- [15] H. Yetkin, S. Kalouche, M. Vernier, G. Colvin, K. Redmill and U. Ozguner, "Gyroscopic Stabilization of an Unmanned Bicycle," in *American Control Conference*, Portland, USA, 2014.
- [16] S. C. Chapra and R. P. Canale, *Numerical Methods for Engineers*, McGraw-Hill, 2009.
- [17] D. E. Oku and E. P. Obot, "Comparative Study Of PD, PI And PID Controllers For Control Of A Single Joint System In Robots," *The International Journal of Engineering and Science (IJES)*, vol. VII, no. 9, pp. 51-54, 2018.
- [18] C. Gurrisi, R. Seidel, S. Dickerson, S. Didziulis, P. Frantz and K. Ferguson, "Space Station Control Moment Gyroscope Lessons Learned," *Proceedings of the 40th Aerospace Mechanisms Symposium*, pp. 161-176, 2010.
- [19] N. S. Nise, "Chapter 4: Time Response," in *CONTROL SYSTEMS ENGINEERING Sixth Edition*, Pomona, John Wiley & Sons, Inc., 2011, pp. 161-214.
- [20] K. Ogata, "ZIEGLER–NICHOLS RULES FOR TUNING PID CONTROLLERS," in *Modern Control Fifth Edition*, New Jersey, Prentice Hall, 2010, pp. 568-571.

APPENDIX I: PYTHON CODE FOR CONTROLLED SYSTEM

```
#!/usr/bin/env python

import os
import matplotlib.pyplot as plt
import numpy as np
import differential_equations

# All units are in SI with exception to degrees which are used
# in plotting graphs.
# Gyroscope parameters
largest_gyro_length = 11.4
rod_rad = 1 * 10**-2
disk_rad = np.sqrt(4 / 5) * largest_gyro_length * 10**-2
rod_len = np.sqrt(4 / 5) * largest_gyro_length * 10**-2
# rod_len = 10*10**-2
disk_len = rod_len
# disk_pos = 6.5*10**-2
disk_pos = 0
density = 7.85 * 10**3

# mass of gyroscope calculations
# gyro_mass = density*np.pi*(rod_rad**2*rod_len+(disk_rad**2-
# rod_rad**2)*disk_len)
gyro_mass = 6.2155

# center of mass of gyroscope calculations
# x_mass_centre = (density*np.pi/gyro_mass)*(rod_rad**2*rod_len**2/2+
# (disk_rad**2 \
# -rod_rad**2)*disk_len*(disk_pos+disk_len/2))
#
# Moment of inertia of gyroscope about endpoint of shaft
# I_endpoint = density*np.pi*(rod_rad**4*rod_len/4+((disk_rad**4-rod_rad**4) \
# *disk_len/4)+(rod_rad**2*rod_len**3)/3+(disk_rad**2*rod_rad**2) \
# *(disk_len**3+3*disk_pos**2*disk_len+3*disk_len**2*disk_pos)/3)

# Moment of inertia of gyroscope about center of mass using parallel axis theorem
# This moment of inertia is about both alpha and zeta axis.
# I_xi_xi = I_endpoint - gyro_mass*x_mass_centre**2
I_xi_xi = 0.03509464

# This moment of inertia is about both phi axis.
```

```

#  $I_{\phi\phi} = (1/2)*density*np.pi*(disk\_len*disk\_rad**4-(rod\_len-disk\_len)*rod\_rad**4)$ 
I_phi_phi = 0.067557

# mass of bike(100kg) plus addition payload such as weight of people and other things.
bike_mass = 180
grav_accel = 9.81
# center of mass of bike plus payload just chosen to be at saddle of bike as
# center of mass will be around that position
# Just a rough approximation
bike_mass_center = 0.3

# The position where gyroscope is pivoted. This position is assigned relative
# to
# the ground.
gyro_pos = 0.45
# position where pivot is located on the shaft relative to endpoint of shaft o
f
# gyroscope
pivot_pos = 1 * 10**-2
# length from pivot to gyroscope center of mass
# pivot_len = x_mass_centre-pivot_pos
pivot_len = 0
# angular velocity of gyroscope about phi axis in radian/s
gyro_vel = 500
# number of iterations
iter_num = 30000
# moment of inertia of bike plus that of payload
# estimated as modeling people as bars
# Calculated bike moment of inertia using coding software and finding
# approximate radius of gyration.
I_bike = 30

# initial conditions
# difference between time interval of individual iterations
time_diff = 0.001
# Starting time
init_time = 0
# electrical constants associated with side motor circuit
motor_torque_const = 1.875
back_emf_const = 0.096
inductance = 0.000119
resistance = 0.61
# initial condition matrix 1st entry is that of independent variable latter
# corresponds to dependent variables

```

```

init_cond = np.array([init_time, 0.31, 0, 0])
# conjugate momentum in phi
momentum_phi = I_phi_phi * (gyro_vel + init_cond[2] * np.sin(init_cond[3]))

# constants
oscillation_const = (((bike_mass * grav_accel * bike_mass_center) +
                      (2 * gyro_mass * grav_accel * gyro_pos)) /
                      (2 * I_phi_phi * gyro_vel)) + 15

damping_const = (np.sqrt(
    (I_bike + 2 * gyro_mass * gyro_pos**2) *
    ((2 * I_phi_phi * gyro_vel) * (oscillation_const) -
     (bike_mass * grav_accel * bike_mass_center +
      2 * gyro_mass * grav_accel * gyro_pos))) / (I_phi_phi + gyro_vel)) + 5

proportional_const = 1.8

# functions corresponding to differential equations

def del_theta(x_input):
    """This function corresponds to derivative of theta."""
    theta_dot = x_input[2]
    return theta_dot

def del_theta_dot(x_input):
    """This function corresponds to second derivative of theta."""
    # This if elif statement is used as to allow both one and
    # two dimension array input, as two dimension array computation
    # is useful in graphs
    if x_input.ndim == 1:
        theta = x_input[1]
        theta_dot = x_input[2]
        alpha = x_input[3]
        alpha_dot = del_alpha(x_input)
    elif x_input.ndim == 2:
        theta = x_input[:, 1]
        theta_dot = x_input[:, 2]
        alpha = x_input[:, 3]
        alpha_dot = del_alpha(x_input)

    bike_weight_torque = bike_mass * grav_accel * bike_mass_center * np.sin(
        theta)
    gyro_weight_torque = 2*gyro_mass*grav_accel*(gyro_pos
                                                + pivot_len*np.cos(alpha)) \

```

```

        * np.sin(theta)

restoring_torque = 2 * momentum_phi * np.cos(alpha) * alpha_dot
other_torque = 4 * (I_xi_xi*np.cos(alpha)+gyro_mass
                     * (gyro_pos+pivot_len*np.cos(alpha))*pivot_len) \
               * theta_dot*alpha_dot*np.sin(alpha)

effec_inertia = I_bike+2*gyro_mass*(gyro_pos+pivot_len*np.cos(alpha))**2 \
               + 2*I_xi_xi*(np.cos(alpha))**2

theta_dot_dot = (bike_weight_torque + gyro_weight_torque - restoring_torque + other_torque) / effec_inertia

return theta_dot_dot

def del_alpha(x_input):
    """This function corresponds to derivative of alpha."""
    # This if elif statement is used as to allow both one and two dimension array input, as two dimension array computation is useful in graphs
    if x_input.ndim == 1:
        theta = x_input[1]
        theta_dot = x_input[2]
        alpha = x_input[3]
    elif x_input.ndim == 2:
        theta = x_input[:, 1]
        theta_dot = x_input[:, 2]
        alpha = x_input[:, 3]

    # alpha_dot =(oscillation_const*np.sin(theta)+damping_const*theta_dot \
    #             +proportional_const*alpha)/np.cos(alpha)
    alpha_dot = (oscillation_const * np.sin(theta) + damping_const * theta_dot + proportional_const * alpha)
    return alpha_dot

# solution of differential equations
eqn = differential_equations.DifferentialEquations(del_theta, del_theta_dot, del_alpha)

# solution matrix
solution_matrix = eqn.solution_differential_eqn(time_diff, iter_num, init_cond)

# this function corresponds to torque calculations

```

```

theta_dot_dot_mat = del_theta_dot(solution_matrix)
alpha_dot_mat = del_alpha(solution_matrix)
momentum_phi_mat = momentum_phi * np.ones(len(solution_matrix[:, 0]))

def del_alpha_dot(x_input):
    """This function corresponds to second derivative of alpha."""
    theta = x_input[:, 1]
    theta_dot = x_input[:, 2]
    theta_dot_dot = theta_dot_dot_mat
    alpha_dot = alpha_dot_mat

    #     alpha_dot_dot=(oscillation_const*np.cos(theta)*theta_dot \
    #                 +damping_const*theta_dot_dot+proportional_const*alpha_dot \
    #                 +(alpha_dot**2)*np.sin(alpha))/np.cos(alpha)

    alpha_dot_dot = (oscillation_const * np.cos(theta) * theta_dot +
                    damping_const * theta_dot_dot +
                    proportional_const * alpha_dot)
    return alpha_dot_dot

def del_phi_dot(x_input):
    """This function corresponds to second derivative of phi."""
    theta_dot = x_input[:, 2]
    theta_dot_dot = theta_dot_dot_mat
    alpha = x_input[:, 3]
    alpha_dot = alpha_dot_mat

    phi_dot_dot = - theta_dot_dot \
        * np.sin(alpha)-theta_dot*alpha_dot*np.cos(alpha)
    return phi_dot_dot

alpha_dot_dot_mat = del_alpha_dot(solution_matrix)

def torque(x_input):
    """This function finds the required torque on the gyroscope."""
    theta = x_input[:, 1]
    theta_dot = x_input[:, 2]
    alpha = x_input[:, 3]
    alpha_dot_dot = alpha_dot_dot_mat

    mass_torq = gyro_mass*pivot_len*(gyro_pos+pivot_len*np.cos(alpha)) \
        * np.sin(alpha)*theta_dot**2

```

```

restoring_torq = momentum_phi * theta_dot * np.cos(alpha)
inertia_torq = I_xi_xi * theta_dot**2 * np.cos(alpha) * np.sin(alpha)
weight_torq = gyro_mass*grav_accel*pivot_len*np.sin(alpha) \
* np.cos(theta)

effec_inertia = gyro_mass * pivot_len**2 + I_xi_xi

torque_mat = effec_inertia*alpha_dot_dot \
- (-mass_torq+restoring_torq-inertia_torq+weight_torq)
return torque_mat

torque_mat = torque(solution_matrix)

def energy(x_input):
    """This is energy function of the system."""
    theta = x_input[:, 1]
    theta_dot = x_input[:, 2]
    alpha = x_input[:, 3]
    alpha_dot = alpha_dot_mat
    momentum_phi = momentum_phi_mat

    energy_mat = (1/2)*I_bike*theta_dot**2 \
        + gyro_mass*((gyro_pos+pivot_len*np.cos(alpha))**2)*theta_dot**2) \
        + I_xi_xi*(np.cos(alpha)*theta_dot)**2 \
        + (gyro_mass*pivot_len**2+I_xi_xi)*(alpha_dot**2) \
        + (momentum_phi**2/I_phi_phi) \
        + bike_mass*grav_accel*bike_mass_center*np.cos(theta) \
        + 2*gyro_mass*grav_accel*(gyro_pos+pivot_len * \
            np.cos(alpha))*np.cos(theta)
    return energy_mat

def phi_dot(x_input):
    """This function corresponds to derivative of phi."""
    theta_dot = x_input[:, 2]
    alpha = x_input[:, 3]
    momentum_phi = momentum_phi_mat
    phi_dot_mat = (momentum_phi / I_phi_phi) - theta_dot * np.sin(alpha)
    return phi_dot_mat

def momentum_theta(x_input):
    """This function corresponds to conjugate momentum for theta."""

```

```

theta_dot = x_input[:, 2]
alpha = x_input[:, 3]

momentum_theta_mat = I_bike*theta_dot \
+ 2*gyro_mass*((gyro_pos+pivot_len*np.cos(alpha))**2)*theta_dot \
+ 2*momentum_phi*np.sin(alpha)+2*I_xi_xi \
* ((np.cos(alpha))**2)*theta_dot

return momentum_theta_mat

def momentum_alpha():
    """This function corresponds to conjugate momentum for alpha."""
    alpha_dot = alpha_dot_mat
    return (I_xi_xi + gyro_mass * pivot_len**2) * (alpha_dot)

def del_energy(x_input):
    """This function corresponds to 2*integral of torque wrt alpha."""
    return 2 * np.sum(torque_mat[:-1] * (x_input[1:, 3] - x_input[:-1, 3]))

current = torque_mat / motor_torq_const
del_current = np.zeros(len(current))
del_current[:-1] = (current[1:] - current[:-1]) / time_diff
voltage = inductance*del_current + resistance \
* current + back_emf_const*alpha_dot_mat
# print(del_energy(solution_matrix))
# print(energy(solution_matrix)[iter_num-1] - energy(solution_matrix)[0])

try:
    os.mkdir("gyroscope_forced_graphs")
except:
    pass

try:
    os.chdir('gyroscope_forced_graphs')
except:
    exit()

```

APPENDIX II: RK ORDER 4 METHOD CODE

```
#!/usr/bin/env python
import numpy as np

class DifferentialEquations:
    def __init__(self, *args):
        self.args = args

    def runge_kutta_order_4(self, delta_time, i_th_iteration):
        """
        Calculation of i+1 iteration using range-kutta method.

        This calculating next iteration from values of current iteration
        with help of runge-kutta method of order 4.

        Parameters
        -----
        delta_time : float
            time step between two time iterations.
            delta time is the change in independent variable
            between 2 iterations
        i_th_iteration : array
            values of independent and dependent variables for current iteration
        n
            ith iteration matrix has time in the 0th index and x in 1st index
            and dx/dt in 2nd index and so on.

        """
        # initializing runge kutta constants to be zero matrices. Constant
        # matrices are defined as [ K1 L1 M1 ..... ]
        # Length of runge kutta constants length
        range_kutta_constant_length = len(i_th_iteration)-1
        range_kutta_constant_1 = np.zeros(range_kutta_constant_length)
        range_kutta_constant_2 = np.zeros(range_kutta_constant_length)
        range_kutta_constant_3 = np.zeros(range_kutta_constant_length)
        range_kutta_constant_4 = np.zeros(range_kutta_constant_length)

        # Initialization of i_plus_1_th_iteration matrix
        i_plus_1_th_iteration = np.zeros(len(i_th_iteration))

        # This dummy variable is defined to add i_th_iteration matrix and
        # range kutta constants as the both have different lengths
```

```

dummy_argument = np.zeros(len(i_th_iteration))

# Calculating 1st range kutta constant
for index, arg in enumerate(self.args):
    range_kutta_constant_1[index] = delta_time*arg(i_th_iteration)

# Calculating 2nd range kutta constant
for index, arg in enumerate(self.args):
    dummy_argument[0] = i_th_iteration[0]+delta_time/2
    dummy_argument[1:] = i_th_iteration[1:]+range_kutta_constant_1/2

    range_kutta_constant_2[index] = delta_time*arg(dummy_argument)

# Calculating 3rd range kutta constant
for index, arg in enumerate(self.args):
    dummy_argument[0] = i_th_iteration[0]+delta_time/2
    dummy_argument[1:] = i_th_iteration[1:]+range_kutta_constant_2/2

    range_kutta_constant_3[index] = delta_time*arg(dummy_argument)

# Calculating 4th range kutta constant
for index, arg in enumerate(self.args):
    dummy_argument[0] = i_th_iteration[0]+delta_time
    dummy_argument[1:] = i_th_iteration[1:]+range_kutta_constant_3

    range_kutta_constant_4[index] = delta_time*arg(dummy_argument)

# i+1 iteration = i iteration + (K1+2*K2+2*K3+K4)/6
# value at index 0 for time is handled appropriately
i_plus_1_th_iteration[0] = i_th_iteration[0]+delta_time

i_plus_1_th_iteration[1:] = i_th_iteration[1:] \
    + (range_kutta_constant_1+2*range_kutta_constant_2 \
    + 2*range_kutta_constant_3+range_kutta_constant_4)/6

return i_plus_1_th_iteration

def solution_differential_eqn(self, delta_time, iter_num, init_cond):
    """
    Solving differential equation using runge kutta method of order 4.

    The final solution matrix has each row representing each
    iteration. The column represent variables. The zeroth column is
    time, first is x, second is dx/dt.
    """

    Parameters
    -----

```

```

delta_time : float
    time step between two time iterations.
iter_num : int
    total number of iterations to be performed.
init_cond : array
    initial conditions for the differential equation.
"""

# starting point for 1st iteration
i_th_iteration = init_cond
# solution matrix(rows represent iterations and columns represent variable.
solution = np.zeros([iter_num, len(i_th_iteration)])
# 1st row of solution matrix is set equal to initial conditions
solution[0, :] = init_cond

for i in range(1, iter_num):
    # initial_time=i_th_iteration[0]
    i_th_iteration = self.runge_kutta_order_4(
        delta_time, i_th_iteration)
    solution[i, :] = i_th_iteration
return solution

```

APPENDIX III: MATLAB CODE FOR CONTROLLER

```

m_b      = 180;
R1       = 0.3
m_g      = 6.2155;
r        = 0.45;
l        = 0;
I_b      = 30;
P_phi    = 67.557;
I_alpha_alpha = 0.035094;
I_phi_phi   = 0.067557;
g        = 9.8;
K_t      = 1.875;
K_e      = 0.096;
L        = 0.000119;
R        = 0.61;

%%
A = [0 1 0 0 0; (m_b*g*R1+2*m_g*g*(r+l))/(I_b+2*m_g*r^2+4*m_g*r*l) 0 0
P_phi/(I_b+2*m_g*r^2+4*m_g*r*l) 0;0 0 0 1 0;0
-P_phi/(2*I_alpha_alpha+2*m_g*l^2) m_g*g*l/(I_alpha_alpha+m_g*l^2) 0
K_t/(I_alpha_alpha+m_g*l^2);0 0 0 -K_e/L -R/L]

B = [0;0;0;0;1/L]

C = [1 0 0 0 0]

D = 0

[b,a] = ss2tf(A,B,C,D);

bike = tf([b],[a])

%step(b,a)

%rlocus(bike);

%bode(bike)
%[Gm,Pm,Wgm,Wpm] = margin(bike)

%pzmap(bike);

%%
Kp = 34.3993210896001
Ki = 21.5738802879741
Kd = 2.96718594627602
Kn = 3.68324125230203

bikec = pid(Kp,Ki,Kd,Kn)
%Mc = feedback(bike*bikec,1)
%step(bike)
grid on
%pzmap(bike)

```

```
%pzmap (Mc)
%rlocus (Mc)
%bode (Mc)
%step (Mc)
```

APPENDIX IV: CONTROLLER PARAMETERS

Controller Parameters

	Tuned	Block
P	34.3993	34.3993
I	21.5739	21.5739
D	2.9672	2.9672
N	3.6832	3.6832

Performance and Robustness

	Tuned	Block
Rise time	0.453 seconds	0.453 seconds
Settling time	4.18 seconds	4.18 seconds
Overshoot	11.7 %	11.7 %
Peak	1.12	1.12
Gain margin	6.21 dB @ 44.6 rad/s	6.21 dB @ 44.6 rad/s
Phase margin	87.3 deg @ 3.68 rad/s	87.3 deg @ 3.68 rad/s
Closed-loop stability	Stable	Stable

APPENDIX V: BILL OF MATERIALS

Table 7: Bill of Materials

Components	Price (Rs)
2x Hub Motor	74,896
Battery (48V)	22,000
Tinysine 10 DOF IMU	5,320
Gyroscope Flywheel (Material + Machining)	4,000
SbRIO-9626 Controller	55,000
2x ESCAP 16 Servo Motor with Encoder	5,000
Buffer for electrical components/wires	2,000
8x 6000 Deep Grove Ball bearing	4,000
Total	172,216
Cumulative CG125 (PKR 134,900) with gyro	307,116
Cumulative CD70 (PKR 76,900) with gyro	249,116
Honda Rider Assist (Cheapest)	3,000,000
Savings	89.8% - 91.7%

APPENDIX VI: BEARING DIMENSIONS

Table 8: 6000 Ball Bearing Properties

Properties	Dimensions
Size	10mm x 26mm x 8mm
Bearing Inner Diameter	10mm
Bearing Outer Diameter	26mm
Bearing Width	8mm

APPENDIX VII: DETAILED PART DRAWINGS

